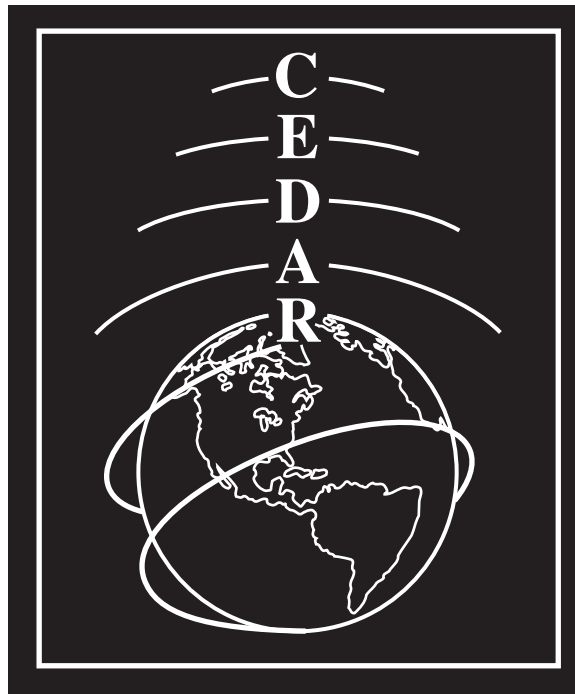


**2003 CEDAR Workshop
Raintree Plaza Conference Center
Longmont, Colorado, USA
June 15-20, 2003**

**Poster Sessions Booklet
June 17-18**



Sponsored by HAO/NCAR and NSF

Contents

1	Tuesday Evening 17 June 2003 Poster Session Abstracts, Polar mesospheric summer echoes (PMSE) / Polar mesospheric clouds (PMC)	1
1.1	PMSE.01: Observations of PMSE using Range Image (RIM) on the EISCAT VHF Radar: Phase Calibration Issues by Fernandez, Jose	1
1.2	PMSE.02: Further observations of PMSE in Antarctica by Sarango, Martin	1
1.3	PMC.01: Polar mesospheric clouds and temperatures measured by the Fe Boltzmann temperature lidar at Rothera, Antarctica by Chu, Xinzhao	2
1.4	PMC.02: Characteristics and dynamics of polar mesospheric clouds by Mackler, David	2
1.5	PMC.03: The Identification and Characterization of Polar Mesospheric Clouds (PMCs) in HALOE data. by Wrotny, Jonathan	2
2	Tuesday Evening 17 June 2003 Poster Session Abstracts, Mesosphere-Lower Thermosphere General Studies	4
2.1	MLT.01: Observed Instability Layers and Diffusivities in the Mesosphere and Lower Thermosphere During the TOMEX Experiment by Bishop, Rebecca	4
2.2	MLT.02: Mesospheric Temperature Climatology from a Mid-Latitude Lidar Site in the Rocky Mountains by Herron, Joshua	4
2.3	MLT.03: Wintertime Atmospheric Temperature Structure from the ground to 110 km at Syowa Station (39E, 69S) by Kawahara, Taku	4
2.4	MLT.04: High-resolution observations of mesospheric dynamics with the 50 MHz Jicamarca radar by Lehmacher, Gerald	5
2.5	MLT.05: Sampling the NCAR TIME-GCM and GSWM for TIMED and CEDAR related studies and preliminary model/observation intercomparisons by Oberheide, Jens	5
2.6	MLT.06: Lidar observations of the high-latitude summertime sodium layer in the presence of noctilucent clouds at Sondrestrom by Pan, Weilin	5
2.7	MLT.07: Observations of Winds and Momentum Fluxes in the Lower Thermosphere over Arecibo by Riggins, Dennis M.	6
2.8	MLT.08: All sky airglow imaging observations of "dark streaks" over Clemson: Is it a bore? by Brown, Bailes	6
2.9	MLT.09: SABER Observations of Polar Summer and Polar Winter Mesospheric and Lower Thermospheric Temperatures and Comparisons with Correlative Measurements Taken During the MaCWAVE Campaign by Mertens, Christopher	6
2.10	MLT.10: An intercomparison of winds measured by falling sphere, Weber sodium lidar, and meteor radar during the summer 2002 MaCWAVE/MIDAS and the winter 2003 MaCWAVE campaigns by Vance, J	7
2.11	MLT.11: Monte-Carlo Simulation of Vertical Heat Flux Measurements by Sodium Doppler Wind/Temperature Lidar by SU, LIGUO	7
2.12	MLT.12: Summer polar mesopause region temperatures measured in 2001 by the ALOMAR Weber Sodium Lidar by Williams, Bifford	8
2.13	MLT.13: The Reactions of Ionic Iron in the Upper Atmosphere by Woodcock, Kenneth	8
2.14	MLT.14: New NCAR Fabry-Perot interferometer Neutral Wind Observation by Wu, Qian	9
2.15	MLT.15: Comparison of TIMED/SABER Non-LTE Temperature Retrievals with Ground-Based Mesospheric Temperature Mapper Measurements by Zhao, Yucheng	9
3	Tuesday Evening 17 June 2003 Poster Session Abstracts, Mesosphere-Lower Thermosphere Gravity Waves	10
3.1	GWV.01: THE MESOSPHERE-THERMOSPHERE NIGHTGLOW SENSITIVITY TO TECTONIC EVENTS by Didebulidze, G.G.	10
3.2	GWV.02: SHORT-PERIOD ATMOSPHERIC GRAVITY WAVES AMPLITUDE AMPLIFICATION ON MAGNETICALLY DISTURBED DAYS AT THE MESOSPHERE-THERMOSPHERE HEIGHTS by Didebulidze, G.G.	10

3.3	GWV.03: Comparison of wind velocity between MU radar and FPI — possible effect of OI5577 airglow height variation — by Fujii, Junsuke presented by Nakamura, Takuji	11
3.4	GWV.04: Height variation of OI5577 airglow observed by dual site all-sky imagers by Fukushima, Tetsuya presented by Nakamura, Takuji	11
3.5	GWV.05: Antarctic Observations on Hydroxyl Airglow. by French, John	11
3.6	GWV.06: Simultaneous Mesospheric Wind, Gravity Wave and Temperature Measurements at Bear Lake Observatory, Utah (41.6 N) by Hatch, D.	12
3.7	GWV.07: High Frequency Gravity Wave Damping in the Mesopause Region from Airglow Measurements at Albuquerque, New Mexico by Li, Feng	12
3.8	GWV.08: Low-Frequency Tropospheric Forcing as a Source of Quasi-Monochromatic Gravity Waves Observed in the Upper Mesosphere and Lower Thermosphere by Snively, Jonathan	13
3.9	GWV.09: Extraction of Gravity Wave Momentum Fluxes From Airglow Images by Tang, Jing	13
3.10	GWV.10: Five Minutes Gravity Waves due to Thunderstorm Activity in the Gulf of Mexico. by Martinez, Lisandro	14
3.11	GWV.11: Airborne Investigations of Atmospheric Emissions (0.9–1.6 microns) using an InGaAs Camera by Nielsen, Kim	14
3.12	GWV.12: Equatorial MLT Gravity Wave Measurements by Olsen, Christian	14
3.13	GWV.13: Multi-Diagnostic Measurements of a Large Gravity Wave Event at Arecibo Observatory, Puerto Rico. by Smith, Steve	15
3.14	GWV.14: GRAVITY WAVE PROPAGATION MEASURED IN BRAZILIAN EQUATORIAL AND MIDDLE LATITUDE REGION by Wrasse, Cristiano	15
3.15	GWV.15: Characteristics of inertio-gravity waves in the upper troposphere and lower stratosphere over the South Pacific as revealed by GPS radiosondes by Yamamori, Miho	15
3.16	GWV.16: A Full-Wave Investigation of the Use of a 'Cancellation Factor' in GW-Airglow Interaction Studies by Yu, Yonghui	16
4	Tuesday Evening 17 June 2003 Poster Session Abstracts, Other waves (tidal, planetary, small scale, etc.)	17
4.1	OWV.01: Variability in the mesosphere and ionosphere during the April 2002 by Goncharenko, Larisa	17
4.2	OWV.02: Small-Scale Wave Structures in OH Airglow and Simultaneous Na Lidar Instability Observations by Li, Tao	17
4.3	OWV.03: Interannual and subseasonal variability of diurnal tides and tropospheric diurnal heating by Lieberman, Ruth	17
4.4	OWV.04: Quasi-two-day variations observed by airglow and meteor wind in the equatorial region by Lima, Lourivaldo Mota	18
4.5	OWV.05: Impact of Lower Atmosphere Forcing on Electrodynamical Variability in the Equatorial Ionosphere and Thermosphere by Maruyama, Naomi	18
4.6	OWV.06: Investigations of the 8-hr wave in the mesosphere and thermosphere by Mutiso, Charles	19
4.7	OWV.07: Identifying tides and planetary waves in night-time LIDAR data using the Lomb-Scargle periodogram by Nelson, Karen	19
4.8	OWV.08: Mean wind and atmospheric tide observed at Tromsø and Poker Flat by Nozawa, Satonori	19
4.9	OWV.09: INVESTIGATING MESOSPHERIC OH AND O ₂ TEMPERATURE VARIABILITY AT LOW LATITUDES OVER MAUI, HAWAII. by Taori, A	20
4.10	OWV.10: Yearlong Na-Lidar observation of temperature and winds over full diurnal cycles above Ft. Collins, CO (40N, 105W) by Yuan, Tao	20
4.11	OWV.11: Interpretation of apparent storm-related effects in the mesosphere at high latitudes during April 2002. by Zhang, Shengpan	21
4.12	OWV.12: Seasonal, annual, and long-term airglow emission rate variabilities in the mesosphere and lower thermosphere observed by WINDII during 1990's by Zhang, Shengpan	21

4.13	OWV.13: Nonmigrating Tides as Measured by the SABER Instrument on TIMED during April, 2002: The Aliasing Problem by Zhang, Xiaoli	22
5	Tuesday Evening 17 June 2003 Poster Session Abstracts, Instruments and techniques for middle atmospheric and ionosonde observations	23
5.1	IMI.01: The SHIMMER Instruments: Spatial Heterodyne Imagers for Remote Sensing of the Atmosphere from Space by Englert, Christoph R.	23
5.2	IMI.02: A Stereoscopic imaging method for measuring the altitude of the near infrared airglow layer by Faivre, Michael	23
5.3	IMI.03: Microcontroller-Based Closed-Loop Laser Tuning System by Peshave, Manasi	24
5.4	IMI.04: Application Of The Ucar-stars Method To MF Radars by Praskovskaya, Eleanor . .	24
5.5	IMI.05: The structure function-based approach to data analysis for spaced antenna radars: a comparison with traditional techniques by Praskovsky, Alexander	25
5.6	IMI.06: Co-located Instruments Simulation by Vemula, Sreenivas	25
5.7	IMI.07: Rayleigh Lidar Measurements of Temperature and Density by Wang, Weiyuan . . .	25
5.8	IMI.08: A Real-Time Preview of the 21st Century Ionosonde by Wright, John	26
6	Tuesday Evening 17 June 2003 Poster Session Abstracts, Meteor science (other than winds)	27
6.1	MET.01: Observations of meteor-head echoes using the Jicamarca 50 MHz radar in interferometer mode by Chau, Jorge L.	27
6.2	MET.02: Observations of Sporadic Meteor Events Using the 430 MHz Arecibo Radar by Briczinski, Stanley	27
6.3	MET.03: Meteoric dust effects on Mesospheric Electrodynamics by Gelinas, Lynette	27
6.4	MET.04: Simulations of Large-Aperature Radar Meteor Observations by Ray, Licia	28
6.5	MET.05: Signal Processing Techniques for Bursty Interference Removal by Wen, Chun-Hsien	28
7	Tuesday Evening 17 June 2003 Poster Session Abstracts, Lightning / Sprites	29
7.1	LSP.01: Multi-path D region ionospheric remote sensing by Cheng, Zhenggang	29
7.2	LSP.02: EXPANSION AND ACCELERATION OF STREAMERS IN SPRITES by Liu, Ningyu	29
7.3	LSP.03: Direction-Finding of Scattered Fields Produced During Non-Ducted LEP Events as Measured at Palmer Station, Antarctica by Moore, Robert	30
8	Tuesday Evening 17 June 2003 Poster Session Abstracts, Stratosphere and below	31
8.1	STR.01: A system study of a troposphere lidar system. by Yue, Jia	31
9	Wednesday Evening 18 June 2003 Poster Session Abstracts, Solar-planetary interactions in the upper atmosphere of Earth and other planets	32
9.1	SPI.01: Examining the effect of different forcing terms to the thermospheric neutral winds by Deng, Yue	32
9.2	SPI.02: The Solar X-ray Imager (SXI) Occultation Experiment by Hill, Steven	32
9.3	SPI.03: Photochemical modeling of global variations and ring shadowing in Saturn's ionosphere by Moore, Luke	32
10	Wednesday Evening 18 June 2003 Poster Session Abstracts, Magnetosphere/ionosphere coupling and plasmasphere	34
10.1	MIC.01: Multivariate Statistical Analysis of Ion Upwelling using Incoherent Scatter Radar Data by Remick, Karen	34
10.2	MIC.02: Modeling Ionosphere-Thermosphere-Magnetosphere Coupling with the IntegratedSpace Weather Prediction Model (ISM) by Schoendorf, J	34
10.3	MIC.03: Comparisons of He+ in the plasmasphere with the CTIP model and EUV data from the IMAGE satellite. by Thom, Stuart	34

11 Wednesday Evening 18 June 2003 Poster Session Abstracts, Long term variations of the upper atmosphere	35
11.1 LTV.01: INITIAL SCIENCE PLANS FOR CAUSES (CLIMATE AND WEATHER OF THE SUN-EARTH SYSTEM): REQUEST FOR IDEAS AND INPUTS by Basu, Sunanda . . .	35
11.2 LTV.02: Online Database for Thermal Ionospheric Plasma Data from DMSP by Hairston, Marc	35
11.3 LTV.03: The analysis of TEC data from TOPEX/Poseidon mission by Jee, Geonhwa	35
11.4 LTV.04: Climatology of Extreme Upper Atmospheric Heating Events by Knipp, Delores . .	36
11.5 LTV.05: Towards a Determination of Thermospheric and Exospheric Hydrogen Densities from Coincident Ground-Based and Satellite Airglow Data by Mierkiewicz, Edwin	36
11.6 LTV.06: Exploration of Trends in the Wisconsin Long Term Record of Thermospheric+Exospheric H-alpha Column Emission Intensities by Nossal, Susan	37
11.7 LTV.07: Long Duration Incoherent Scatter Data Sets by Van Eyken, Tony	38
11.8 LTV.08: Millstone Hill ISR Long-Duration Experiments - Preliminary Analysis by Zhang, Shun-Rong	38
12 Wednesday Evening 18 June 2003 Poster Session Abstracts, Polar dynamics and aeronomy	39
12.1 POL.01: Evaluation of Statistical Convection Patterns For Real-Time Ionospheric Specifications and Forecasts by Bekerat, Hamed	39
12.2 POL.02: Convective behaviour and growth of E-region HF irregularities by Drexler, Josef . .	39
12.3 POL.03: Joule heat calculations, standard deviations, and cross-correlations derived from the Dynamics Explorer-2 satellite by Emery, Barbara	39
12.4 POL.04: Monte Carlo Simulation for the Spreading Effect of an Auroral Proton Beam by Fang, Xiaohua	40
12.5 POL.05: Theoretical Investigation of High-Latitude Outflow for Ions and Neutrals by Gardner, L	41
12.6 POL.06: MESO-SCALE VELOCITY STRUCTURE IN THE HIGH LATITUDE F-REGION by Johnson, Eric	41
12.7 POL.07: Climatological Characteristics of the Polar Ionosphere Based on the Sondrestrom and Chatanika Incoherent Scatter Radar Measurements by Kwak, Young-Sil	41
12.8 POL.08: Ion temperature maximum appeared in the polar E-F transition region by OYAMA, SHIN-ICHIRO	42
12.9 POL.09: High-Latitude Joule Heating Rates Using Different Electric Field Models During the May 1998 Storm by Ridley, Aaron	42
12.10 POL.10: Electrodynamic Characteristics of the Duskside Branch of the Two-Cell Aurora by Shue, Jih-Hong	43
13 Wednesday Evening 18 June 2003 Poster Session Abstracts, Mid-latitude thermosphere and ionosphere	44
13.1 MTI.01: The Sporadic E Layer Instability by Cosgrove, Russell presented by Heinselman, Craig	44
13.2 MTI.02: Thermospheric winds derived from the MU radar incoherent scatter observations by Kawamura, Seiji	44
13.3 MTI.03: Comparison of ionospheric dynamo currents and magnetic perturbations modeled by the TIEGCM with CM3e model results by Maute, Astrid	44
13.4 MTI.04: Implementation of the ionospheric E-region in the Sheffield University Plasmasphere-Ionosphere Model. by Terra, Pedrina	45
14 Wednesday Evening 18 June 2003 Poster Session Abstracts, Equatorial thermosphere and ionosphere	46
14.1 EQU.01: Characterization of Low-Latitude Ionospheric Plasma Depletions Using Space-Based Ultraviolet Imaging by Comberiate, Joseph	46

14.2	EQU.02: Post-Sunset Equatorial Plasma Bubbles During Geomagnetic Storms by Habash Krause, Linda	46
14.3	EQU.03: Equatorial plasma depletions: large-scale structure and scintillation by Hei, Matthew	46
14.4	EQU.04: A Study of the Seasonal Variation of the Low-Latitude Ionosphere by Lin, Charles	47
14.5	EQU.05: Post-sunset equatorial irregularities and magnetic storms by Martinis, Carlos . . .	47
14.6	EQU.06: Horizontal Density Gradient as an Indicator for the Subsequent Occurrence of Equatorial Spread-F Irregularities Along a Satellite Track at 600 km Altitude by Su, Shin-Yi presented by Ho, Hsu-Hui	48
14.7	EQU.07: The Seasonal and Local-time Variations of the Global Topside Ionospheric ion Density at 600 km Altitude and its Relationship to the Occurrence Rate of the Equatorial Spread-F Irregularities by Su, Shin Yi presented by Huang, Chiung Huie	48
14.8	EQU.08: Statistics of equatorial Spread F activity during the June solstice in the American sector by Valladares, Cesar	49
14.9	EQU.09: Longitude variations in topside equatorial ionospheric parameters and comparisons with ground based radars by Venkatraman, Sarita	49
15	Wednesday Evening 18 June 2003 Poster Session Abstracts, Instruments/techniques for thermosphere and ionosphere observations	50
15.1	ITI.01: New All-Sky Imager and Microbarograph at Arecibo Supports CEDAR Community. by Farias Gutierrez, Paloma	50
15.2	ITI.02: Preliminary Analysis of Data Gathered from the New All-sky Imager and Microbarograph System at AO. by Wiig, Johannes	50
15.3	ITI.03: Observation and Analysis of Whistler Mode Echoes Received by RPI on IMAGE at High Latitudes by Chen, Xiangdong	50
15.4	ITI.04: Instrumentation upgrade for Fabry-Perot studies of equatorial thermospheric dynamics and composition by Chen, Xiangdong	51
15.5	ITI.05: SOFDI: An Update on Instrument Development, Forward Model, and Inversion Algorithms by Gerrard, Andrew	51
15.6	ITI.06: A Microcontroller based Generic Radar Controller by Kolatkar, Aditi	52
15.7	ITI.07: Application of Neural Network for Ionospheric Data Assimilation and Forecasting by Mantz, Chris	52
15.8	ITI.08: A new lagprofile based approach to the inversion of incoherent scatter radar data by Nikoukar, Romina	52
15.9	ITI.09: Identification of Ionospheric Sporadic E using Fuzzy Equivalence Techniques by SIKDAR, PAYEL	53
15.10	ITI.10: Calculating induced electric and magnetic fields near coastal regions by Simon, Shepherd	53
15.11	ITI.11: Effects of hot oxygen on midlatitude ground-based Fabry-Perot temperature measurements by Sipler, Dwight	54
16	Wednesday Evening 18 June 2003 Poster Session Abstracts, Data visualization and management	55
16.1	DVM.01: The CEDAR Database by Barnes, Roy	55
16.2	DVM.02: Road map of the TIMED Science Data System web site by Nylund, Stuart	55
16.3	DVM.03: Advances in the Madrigal Database by Rideout, William	55
16.4	DVM.04: Web-Based Space Physics Metadata Searching Using Space Physics Data Markup Language by Weiss, Michele	56
16.5	DVM.05: A Virtual Observatory for the Ionosphere Thermosphere and Mesosphere community by Yee, Jeng-Hwa presented by Nylund, Stuart	56

1 Tuesday Evening 17 June 2003 Poster Session Abstracts, Polar mesospheric summer echoes (PMSE) / Polar mesospheric clouds (PMC)

1.1 PMSE.01: Observations of PMSE using Range IMage (RIM) on the EISCAT VHF Radar: Phase Calibration Issues by Fernandez, Jose

Status of first author: student in poster competition PhD

Authors: J. R. Fernandez jose@doppler.unl.edu Department of Electrical Engineering, University of Nebraska, Lincoln, NE 68588-0511, USA

R. D. Palmer bpalmer@unl.edu Department of Electrical Engineering, University of Nebraska, Lincoln, NE 68588-0511, USA

P. B. Chilson Phillip.Chilson@noaa.gov NOAA Environmental Technology Laboratory, Boulder, CO 80305-3328, USA

I. Haggstrom ingemar@eiscat.com EISCAT Scientific Association, Box 164, S-98123 Kiruna, Sweden

M. Rietveld Mike.Rietveld@eiscat.uit.no EISCAT Scientific Association, Ramfjordmoen, N-9020 Tromsø, Norway

Abstract: A novel phase calibration technique for use with the multiple-frequency Range IMaging (RIM) technique is introduced based on genetic algorithms. The method is used on data collected with the EISCAT VHF radar during a 2002 experiment with the goal of characterizing the vertical structure of Polar Mesosphere Summer Echoes (PMSE) over Norway. Due to the multi-static design of the EISCAT radar, initial phase offsets are present in the multiple-frequency data, which significantly degrade RIM imaging results if not properly calibrated. Using an enhanced numerical simulation method, where data from multiple gates are simultaneously generated, the proposed method is validated. Subsequently, the method is applied to preliminary data from the EISCAT experiment providing first results of RIM images of PMSE.

1.2 PMSE.02: Further observations of PMSE in Antarctica by Sarango, Martin

Status of first author: non-student

Authors: Martin F. Sarango and Ronald F. Woodman

Jicamarca Radio Observatory, Apartado 13-0207, Lima 13, Peru Tel: 51-1-4364978, Fax: 51-1-4344563, e-mail: sarango@jro.igp.gob.pe

Abstract: Here we present and analyze data from the Antarctic summer campaign of 2001. PMSE observations were performed at the Artigas Uruguayan Station (6211S 5854W) using a 15mx15m Yagi array. We compare the results from Artigas with those obtained in previous Antarctic summer campaigns (published or reported at MST conferences). Previously we had used the Machu-Picchu Station radar using a 50mx50m COCO array. Machu-Picchu and Artigas are separated 30 km, both located on King George Is. in Antarctica.

A strong difference in the magnitude of PMSE between the 2001 and the previous campaigns can be observed for the whole season. Furthermore, it is surprising and intriguing that the 10 dB smaller Yagi array at Artigas (250 m²) detected stronger echoes than the COCO array at Machu-Picchu (2500 m²). Although it is well known that a Yagi array can be more efficient than a COCO array of similar dimensions, we have found, from calibration experiments that this is not enough to explain such a discrepancy.

We have two alternatives to explain these differences: 1) unexpected Machu-Picchu poor performance characteristics of the COCO array that have not been accounted for; or 2) an inter-annual variability in the scattering phenomena (i.e., PMSE).

There are two arguments against the first alternative: 1) we have analyzed Stratosphere-Troposphere power data from Machu-Picchu and Artigas and have found that echo strengths are very similar for the two radars; and 2) the results are similar for the four different antenna systems that we have used at Machu-Picchu; i.e., the three original pointing directions and the new vertical array installed in 1998.

The second alternative is somewhat controversial. Arguments against are: 1) Machu-Picchu observations from 1993 to 1999 do not show significant echo strength differences between campaigns; and 2) annual variation in PMSE have not observed from the Poker Flat data base (B. Balsley personal communications). On the other hand, in favor of the annual variability alternative are the results from Svalbard radar in the Northern hemisphere (K. Kubo and J. Roettger personal communications), that reports a 10 dB stronger reflectivity from the 2000 PMSE season with respect to the 1999 and 2001 seasons. Other evidence of long-term variation of mean yearly occurrence of PMSE has been published by Bremer et al., 2003 from Alomar SOUSY (1994-1997) and ALWIN (1999-2001) data bases. Additional shocking results are reported from Resolute Bay (Huaman et al.)(75N,95W). They have found weaker PMSE than those from Poker Flat that could be explained by annual variations of the phenomena. The annual variability alternative would have to be corroborated with new coordinated observations in both the Northern and Southern hemispheres.

1.3 PMC.01: Polar mesospheric clouds and temperatures measured by the Fe Boltzmann temperature lidar at Rothera, Antarctica by Chu, Xinzhao

Status of first author: non-student

Authors: Xinzhao Chu, Graeme Nott*, Patrick Espy*, Chester S. Gardner, Jan Diettrich*, David Maxfield*, Mark Clilverd*, Martin Jarvis*

Department of Electrical and Computer Engineering, University of Illinois at Urbana-Champaign, 1308 West Main Street, Urbana, IL 61801, USA * Physical Science Division, British Antarctic Survey, High Cross, Madingley Road, Cambridge, CB3 0ET, UK

Abstract: After making successful measurements at the North and South Poles, the University of Illinois Fe Boltzmann temperature lidar was relocated to Rothera, Antarctica (67.5 S, 68.0 W) in collaboration with British Antarctic Survey in the summer season of 2002-2003 for the study of polar atmosphere. We report the initial results on polar mesospheric clouds (PMC) and temperatures. Compared with the South Pole, the PMC at Rothera have much lower occurrence probability and much weaker brightness, probably due to the warmer temperatures in summer. The PMC altitudes are around 84.5 km, which are similar to the South Pole PMC and much higher than their northern hemisphere counterparts.

1.4 PMC.02: Characteristics and dynamics of polar mesospheric clouds by Mackler, David

Status of first author: student in poster competition Masters

Authors: David Mackler Embry-Riddle Aeronautical University macklerd@erau.edu

Abstract: The poster will describe the general characteristics of observed PMCs, or more commonly referred as noctilucent clouds. It will also describe observed and theoretical dynamical phenomenon as well as factors that have driven PMC occurrence to increase over the last few decades. Finally it will describe why PMC research is important and the recent areas of interest.

1.5 PMC.03: The Identification and Characterization of Polar Mesospheric Clouds (PMCs) in HALOE data. by Wrotny, Jonathan

Status of first author: student in poster competition PhD

Authors: Jonathan E. Wrotny and Dr. James M. Russell III / Department of Physics, Center for Atmospheric Sciences, Hampton University / jonathan.wrotny@hamptonu.edu and james.russell@hamptonu.edu

Abstract: Data from the Halogen Occultation Experiment (HALOE) are being used to identify and characterize the physical properties of polar mesospheric clouds (PMCs). This analysis is accomplished using the 22 polar summer seasons (11 northern and 11 southern hemisphere) seen by HALOE. Several algorithms are described that screen the HALOE data for PMCs and results of these analyses are presented. In particular,

the number of PMCs and occurrence frequency per season is shown. Several properties of the clouds are also presented including the altitude and latitude distribution of the clouds and the categorization of the cloud extinction at two infrared wavelengths. The possible changes in PMC extinction over time are investigated. The distributions of PMCs over time and spatial coordinates show good agreement with other satellite studies of PMCs such as SME, SNOE, and SBUV. The irregular sampling pattern of HALOE, however, can induce trends and patterns in the plots that are artifacts. Techniques for how to deal with these sampling problems are addressed.

2 Tuesday Evening 17 June 2003 Poster Session Abstracts, Mesosphere-Lower Thermosphere General Studies

2.1 MLT.01: Observed Instability Layers and Diffusivities in the Mesosphere and Lower Thermosphere During the TOMEX Experiment by Bishop, Rebecca

Status of first author: non-student

Authors: R.L. Bishop, Clemson University, rbishop@clemson.edu M.F. Larsen, Clemson University, mlarsen@clemson.edu J.H. Hecht, Aerospace Corporation, James.H.Hecht@aero.org A.Z. Liu, University of Illinois, liuzr@uiuc.edu C.S. Gardner, University of Illinois, cgardner@uillinois.edu

Abstract: The 2000 Turbulent Oxygen Mixing Experiment (TOMEX) combined measurements from rocket-borne instruments and a chemical release experiment with ground-based Na Wind/Temperature lidar measurements to allow a detailed investigation of atmospheric conditions between 80 and 140 km. Lidar measurements over the course of the evening show the evolution of atmospheric stability. At the time of the rocket launch, regions of convective and dynamical instabilities were found to exist. Using the horizontal expansion of the chemical tracer, the estimated diffusivities above 110 km are consistent with molecular diffusion. Below 103 km the corresponding diffusivities are strongly controlled by the instabilities present. The diffusivities measurements suggests that eddy diffusion continues to occur for five to seven kilometers above the nominal turbopause height of 103 km.

2.2 MLT.02: Mesospheric Temperature Climatology from a Mid-Latitude Lidar Site in the Rocky Mountains by Herron, Joshua

Status of first author: student in poster competition PhD

Authors: Joshua P. Herron, Utah State University, joshua.herron@usu.edu
Vincent B. Wickwar, Utah State University, vincent.wickwar@usu.edu

Abstract: Mesospheric temperature climatology has been obtained by Rayleigh-scatter lidar from the Atmospheric Lidar Observatory (ALO) operated by Utah State University (41.7 N, 111.8 W). These temperatures span the region from 45 to 90 km and the period from 1993 till the present. In particular the temperatures from ALO are compared to other ground based instruments.

2.3 MLT.03: Wintertime Atmospheric Temperature Structure from the ground to 110 km at Syowa Station (39E, 69S) by Kawahara, Taku

Status of first author: non-student

Authors: Taku Kawahara, Shinshu University, kawahara@lamar.colostate.edu Alan Z. Liu, University of Illinois at Urbana-Champaign, liuzr@uiuc.edu Weilin Pan, SRI International, weilin.pan@sri.com Chester S. Gardner, University of Illinois at Urbana-Champaign, cgardner@uiuc.edu

Abstract: By combining balloon and Na/Rayleigh temperature lidar data at Syowa station (69S), temperature structure from late Mar to early Oct in 2000/2001 has been characterized from 0 to 110 km. The data are also compared with the temperature model at South Pole of Pan and Gardner [2003] for the same Antarctic lidar observations in the same period. At Showa the annual amplitude as much as 25 K in the stratosphere is in phase because of ozone heating by solar UV absorption. In the mesosphere, the amplitude as much as 28 K is in opposite phase due to adiabatic cooling/heating effect. In this region, the annual amplitude at Syowa is about 5 K smaller than that of South Pole. This suggests the smaller adiabatic heating/cooling effect is seen at Syowa because Syowa is located in lower latitude. In this paper we will talk more detail about the comparison between Syowa and South Pole temperature structure.

2.4 MLT.04: High-resolution observations of mesospheric dynamics with the 50 MHz Jicamarca radar by Lehmacher, Gerald

Status of first author: non-student

Authors: Gerald Lehmacher — Clemson University — glehmac@clemson.edu Erhan Kudeki — University of Illinois — e-kudeki@uiuc.edu Martin Sarango — Jicamarca Radio Observatory — sarango@jro.igp.gob.pe

Abstract: Abstract: The 50 MHz Jicamarca radar is capable of observing daytime mesospheric echo layers on any given day. They are caused by neutral turbulent processes resulting in small-scale fluctuations of the electron density on top of a larger electron density gradient. Using four beams tilted 2.5 degrees off zenith, horizontal and vertical winds are derived from the Doppler spectrum of radar return signals. The vertical resolution of such measurements has considerably improved over the past decades, from several kilometers now to about 150 meters. At this resolution, layers in the lower mesosphere are resolved as thin as a single range bin, while in the upper mesosphere, wider layers exhibit finer substructures indicative of dynamic instabilities and short-period waves. Variations in the spatial structure and orientation of the scatterers and of the wind field may account for small differences seen in the four beams, which at 75 km altitude are only separated by 6 km.

2.5 MLT.05: Sampling the NCAR TIME-GCM and GSWM for TIMED and CEDAR related studies and preliminary model/observation intercomparisons by Oberheide, Jens

Status of first author: non-student

Authors: J. Oberheide, M.E. Hagan, G. Lu, R.G. Roble (HAO/NCAR) C.Y. She, T. Yuan (Colorado State University) D.M. Riggan (Colorado Research Associates) S.E. Palo (U of Colorado) D. Offermann (U of Wuppertal, Germany)

Abstract: The instruments on the TIMED satellite and a complement of ground based CEDAR instruments provide invaluable diagnostics of mesosphere, lower thermosphere, and E-region ionosphere (MLTI, ca. 60-180 km) forcings, dynamics, and energetics. The interpretation of these diagnostics and elucidation of the impact of the associated processes on the MLTI requires complementary modeling initiatives. We make samples of the NCAR TIME-GCM, and GSWM model outputs available to the community via the web. The model results are sampled in a way to provide winds, temperatures, and trace constituents that would be measured by the TIMED instruments if the satellite flew through the model atmosphere. We also provide an analogous product for the CEDAR ground-based component of TIMED. Preliminary model/observation intercomparisons provide a first assessment of the currently available model simulations.

2.6 MLT.06: Lidar observations of the high-latitude summertime sodium layer in the presence of noctilucent clouds at Sondrestrom by Pan, Weilin

Status of first author: non-student

Authors: Weilin Pan, SRI International, weilin.pan@sri.com Jeff Thayer, SRI International, thayer@sri.com John Livingston, SRI International, john.livingston@sri.com

Abstract: Since 1997, Rayleigh lidar and Na lidar measurements have been conducted simultaneously at Sondrestrom, Greenland to study the arctic middle atmosphere. The summertime lidar observations during the typical NLC season from late June through August are used to characterize the mesospheric sodium layer, the noctilucent cloud backscatter, and the atmospheric temperatures. Under the extreme cold temperature condition around the mesopause region, the uptake of metallic sodium below 90 km was observed during the NLC occurrence, as a result of heterogeneous chemical reactions of metal species in the presence of ice particles.

2.7 MLT.07: Observations of Winds and Momentum Fluxes in the Lower Thermosphere over Arecibo by Riggin, Dennis M.

Status of first author: non-student

Authors: Dennis Riggin, Colorado Research Associates, riggin@colorado-research.com
Qihou Zhou, Miami University of Ohio, zhouq@muohio.edu

Abstract: A dual feed system that was made operational at Arecibo Observatory during 2001 allows the Vincent and Reid technique to be used to measure the horizontal wind (one component), the vertical wind and momentum flux. Observations were made using the 430 MHz radar during the daylight hours of October 22-23, 2001 with an east/west viewing geometry. Data sets were obtained using the coded-long-pulse and double-pulse techniques to evaluate the optimal measurement strategy for future experiments. The observations spanned the upper mesosphere and lower thermosphere (approximately 90-140 km). Statistical uncertainties and possible biases resulting from asymmetries between the Gregorian and line-feed beams are discussed.

2.8 MLT.08: All sky airglow imaging observations of "dark streaks" over Clemson: Is it a bore? by Brown, Bailes

Status of first author: student in poster competition Undergraduate

Authors: Bailes Brown (Department of Physics and Astronomy, Clemson University, bailesb@yahoo.com) and John W. Meriwether (Department of Physics and Astronomy, Clemson University, meriwej@clemson.edu)

Abstract: Observations of airglow emissions provide valuable information about the dynamics of the upper atmosphere. In the work reported here, airglow images at wavelengths of 557.7 (OI) and 840 nm (OH) were taken at the Clemsons Atmospheric Research Laboratory (CARL, lat. 34.7, long. 82.75W) from October 2001 to December 2001. These images were processed in a number of ways including directional calibration, background subtraction, and Van Rhijn correction. This processing was accomplished by using both original code and the Viewer software developed by Dr. Jonathan Makela. Analysis of the 557.7 airglow images revealed several nights with interesting data. The particular focus of our analysis was the results for one night that featured a wave structure observed on October 15, 2001, which consisted of two distinct tracks of decreased intensity spaced 200 km or about 1 hour apart in local time but connected in the form of a "wishbone" structure. Furthermore, this "dark streak" structure was found to move at 65 m/s to the north-east with a spatial width of 10-12 km across each streak. An extended region of decreased airglow intensity followed the second "dark streak". Based on these observations, the wave structure is suggested to be a possible candidate that befits the identification of a "bore" that has been discussed in the literature by Dewan and Picard. In addition to typical bore features, the interesting and rather unique wishbone component of the bore structure propagated across the field of view of the imager, i.e., 300 km over two hours. Aside from this structure, examination of the 557 nm airglow images for the whole night showed that the mesosphere was highly active with numerous waves appearing with a wide range of spatial scales. Examination of the OH airglow images showed that this region of the mesosphere was much less active with no indication of the appearance of the bore structure.

2.9 MLT.09: SABER Observations of Polar Summer and Polar Winter Mesospheric and Lower Thermospheric Temperatures and Comparisons with Correlative Measurements Taken During the MaCWAVE Campaign by Mertens, Christopher

Status of first author: non-student PhD

Authors: Christopher J. Mertens, NASA Langley Research Center c.j.mertens@larc.nasa.gov
Francis J. Schmidlin, NASA Wallops Flight Facility, francis.j.schmidlin@nasa.gov

Bifford P. Williams, Colorado State University, biffw@lamar.colostate.edu
 Richard A. Goldberg, NASA Goddard Space Flight Center richard.a.goldberg@nasa.gov
 Chiao-Yao She, Colorado State University, joeshe@lamar.colostate.edu
 Ellis E. Remsberg, NASA Langley Research Center e.e.remsberg@larc.nasa.gov
 James M. Russell III, Hampton University, james.russell@hamptonu.edu
 Martin G. Mlynczak, NASA Langley Research Center m.g.mlynczak@larc.nasa.gov

Abstract: The Sounding of the Atmosphere using Broadband Emission Radiometry (SABER) experiment derives kinetic temperature (Tk) in the mesosphere and lower thermosphere (MLT) from broadband measurements of CO₂ 15 um limb emission, in combination with measurements of CO₂ 4.3 um limb emission used to derive CO₂ volume mixing ratio. Infrared emissions from the CO₂ ro-vibrational bands are in non-local thermodynamic equilibrium (non-LTE) in the MLT, requiring non-LTE processes to be accurately modeled in the retrieval algorithm. In this paper we focus on Tk and show results derived from the non-LTE retrieval algorithm. We demonstrate the ability to retrieve Tk in an extreme non-LTE environment by comparing SABER MLT Tk with rocket falling sphere (FS) and sodium lidar measurements taken during the 2002 summer MaCWAVE campaign. SABER data show a mesopause altitude that changes with latitude and season, consistent with the bimodal character of the mesopause height. We also show preliminary comparisons with the recently available FS and sodium lidar measurements taken during the 2003 winter MaCWAVE campaign.

2.10 MLT.10: An intercomparison of winds measured by falling sphere, Weber sodium lidar, and meteor radar during the summer 2002 MaCWAVE/MIDAS and the winter 2003 MaCWAVE campaigns by Vance, J

Status of first author: student in poster competition PhD

Authors: J.D. Vance B.P. Williams C.Y. She D. Goldberg F. Schmidlin W. Singer R. Latteck

Abstract: The summer MaCWAVE/MIDAS campaign launched a total of 27 falling spheres from rockets between June 29 and July 15, 2002 at Andoya Rocket Range, Norway, followed by the winter MaCWAVE campaign at Esrange, Sweden which launched 37 falling spheres between January 15-30, 2003. The falling spheres measured zonal and meridional winds from 35-89 km altitude. During these campaigns, the Weber sodium lidar at ALOMAR on Andoya, Norway measured zonal winds from 85-97km in summer and 83-100km in winter and the nearby meteor radar on Andoya measured zonal and meridional winds from roughly 82 to 97 km. The falling sphere, lidar and radar winds agreed very well in winter with little mean offset and similar wave patterns. In summer, the three techniques often agreed well, but sometimes the falling spheres and lidar disagreed at 88km with the meteor radar usually splitting the difference.

2.11 MLT.11: Monte-Carlo Simulation of Vertical Heat Flux Measurements by Sodium Doppler Wind/Temperature Lidar by SU, LIGUO

Status of first author: student in poster competition

Authors: 1.LIGUO SU Department of Electrical and Computer Engineering, University of Alaska Fairbanks ftls1@uaf.edu
 2.RICHARD L. COLLINS Department of Electrical and Computer Engineering, University of Alaska Fairbanks rlc@gi.alaska.edu

Abstract: In this poster we will present a Monte Carlo simulation of sodium Doppler wind/temperature lidar measurements. We simulate measurements of vertical wind and temperature in the mesospheric sodium layer. We use a random number generator to model the photon counting errors in the lidar signals. We then use current retrieval methods to derive wind and temperature estimates. We statistically analyze the temperature and wind retrievals to determine the biases and variances in the retrievals. We also determine the biases and variances in the associated wind-temperature flux measurement. We discuss the results in terms of the power-aperture product of the lidar system.

2.12 MLT.12: Summer polar mesopause region temperatures measured in 2001 by the ALOMAR Weber Sodium Lidar by Williams, Bifford

Status of first author: non-student

Authors: B. P. Williams, C. Y. She, J. D. Vance, K. Arnold, P. Acott, D. A. Krueger Physics Department, Colorado State University D. C. Fritts Colorado Research Associates/NWRA

Abstract: Temperature profiles in the mesopause region over Andoya, Norway (69N, 16E) were measured on 18 days during summer 2001, as weather permitted, by the Weber sodium resonance lidar. The daily mean temperatures measured at 87km altitude were generally 10K hotter than rocket falling sphere climatology [Luebken, 1999] compiled from measurements made over 10 years. The transition to higher fall temperatures occurred 2 weeks earlier in the lidar data than the climatology. The difference between the lidar data for 2001 and the falling sphere climatology may be due to interannual variability. The higher temperatures may have implications for PMSE formation, although the large wave perturbations present make interpretation difficult.

2.13 MLT.13: The Reactions of Ionic Iron in the Upper Atmosphere by Woodcock, Kenneth

Status of first author: student not in poster competition PhD

Authors: Kenneth R. S. Woodcock, kenneth.woodcock@uea.ac.uk Tomas Vondrak, t.vondrak@uea.ac.uk John M. C. Plane, j.plane@uea.ac.uk School of Environmental Sciences, University of East Anglia, Norwich, NR4 7TJ, UK.

Abstract: The ablation of, on average, 120 tonnes of interplanetary dust every day is the major source of metal atoms and ions into the Mesosphere and Lower Thermosphere. The reducing environment produced by a high concentration of atomic oxygen, in this region of the atmosphere, results in the formation of a layer of ionic iron above about 90 km. This layer of Fe⁺ ions is maintained from a layer of neutral Fe atoms (at 85-90 km) by solar photo-ionisation and charge transfer with the ambient ions NO⁺ and O₂⁺. Measurements made with rocket-borne mass spectrometry have shown that the most abundant metallic ion above 90 km is Fe⁺, with smaller concentrations of Mg⁺ and Na⁺. Fe⁺ therefore plays a central role in several important plasma-related phenomena. Sporadic E layers being one of these phenomena. Sporadic E layers are thin layers (1-3 km wide), with high concentrations of metallic ions, that occur in the lower thermosphere between 90-120 km. They have a significant impact on radio communications, both by facilitating over-the-horizon HF communication and by obscuring space-to-ground communications, depending on the time of day and the transmission frequency. Above 110 km the Fe⁺ can only be neutralized by the reaction with electrons: Fe⁺ + e⁻ → Fe + hv. This is an inefficient process which, if the only one occurring in the Sporadic E layer, would give it a lifetime of about a day. Below 110 km ion-molecule reactions become more important. Fe⁺ can react with ozone, a very rapid reaction, below 100 km to give: Fe⁺ + O₃ → FeO⁺ + O₂. FeO⁺ undergoes dissociative recombination with an electron to give: FeO⁺ + e⁻ → Fe + O. If these were the only two reactions to occur then the layer would have a lifetime of only a few minutes and not the few hours that have been observed. It has been proposed that atomic oxygen plays an important role in the lifetime of Sporadic E layers by reacting with FeO⁺ to give: FeO⁺ + O → Fe⁺ + O₂. Thus the atomic oxygen continually recycles Fe⁺ slowing down the neutralisation process. As the Sporadic E layer descends the concentrations of O₂, N₂, H₂O and CO₂ increase and these also begin to play a role in the lifetime of the layer. In the presence of a third body (N₂) they react or cluster with Fe⁺ to produce FeO₂⁺, FeN₂⁺, Fe⁺.H₂O and Fe⁺.CO₂. All four compounds can then undergo electron dissociative recombination to give neutral iron or react with atomic oxygen to give Fe⁺. We have used the laser ablation of a rotating iron rod in a fast-flow tube to measure the rate constants of these and a number of other related ion-molecule reactions the rates of which we publish here.

2.14 MLT.14: New NCAR Fabry-Perot interferometer Neutral Wind Observation by Wu, Qian

Status of first author: non-student

Authors: Q. Wu, NCAR, qwu@ucar.edu T. L. Killeen, NCAR S. C. Solomon, NCAR R. D. Gablehouse, NCAR C. Y. She, CSU Y. Tao, CSU

Abstract: Mesospheric and thermospheric neutral wind measurements have been made by a newly built Fabry-Perot interferometer with OH, O 5577A and 6300A emissions at Boulder, Colorado (40 N). The integration times for OH, O 5577 A and 6300 A emissions are 3, 3, and 5 minutes, respectively. The wind errors are 7, 3, and 3-15 m/s for the three emissions. The mesosphere and lower thermosphere neutral winds show clear tidal features. We will also present comparison results with Na lidar from Ft. Collins.

2.15 MLT.15: Comparison of TIMED/SABER Non-LTE Temperature Retrievals with Ground-Based Mesospheric Temperature Mapper Measurements by Zhao, Yucheng

Status of first author: non-student

Authors: Y. Zhao, Center for Atmospheric and Space Sciences, Utah State University yucheng@cc.usu.edu
M. J. Taylor Center for Atmospheric and Space Sciences, Utah State University mtaylor@cc.usu.edu
C. J. Mertens Atmospheric Sciences Division, Chemistry and Dynamics Branch, NASA Langley Research Center c.j.mertens@larc.nasa.gov
J. M. Russell III Center for Atmospheric Sciences, Hampton University james.russell@hamptonu.edu

Abstract: An important goal of the NASA TIMED satellite mission is to map the temperature field of the earth's upper atmosphere (core region 60-180 km) on a global scale. The SABER instrument onboard TIMED uses measurements of the CO₂ limb emissions at 15 m to derive height profiles of atmospheric temperature (altitude 40-135 km) with a vertical resolution of 2 km. As part of a novel program to investigate the dynamics of mesospheric temperature variability at low-latitudes, ground-based measurements using the USU-CEDAR Mesospheric Temperature Mapper (MTM) located at Maui, Hawaii (20.8 N, 156 W) have recently been compared with SABER overpasses within 500 km of the Hawaiian Islands. The MTM utilizes the near infrared OH (6, 2) Meinel and O₂ (0, 1) Atmospheric band nightglow emissions to infer atmospheric temperature at two mean altitudes 87 and 94 km (averaged over 10 km layer FWHM) within the SABER temperature profile. The combination of these two separate measurement techniques provides a powerful and complementary method for investigating temporal and spatial-induced variability. This poster focuses on data from February and July/August 2002 to investigate winter-summer differences and nocturnal variability.

3 Tuesday Evening 17 June 2003 Poster Session Abstracts, Mesosphere-Lower Thermosphere Gravity Waves

3.1 GWV.01: THE MESOSPHERE-THERMOSPHERE NIGHTGLOW SENSITIVITY TO TECTONIC EVENTS by Didebulidze, G.G.

Status of first author: non-student

Authors: G. G. Didebulidze(1), J. F. Kafkalidis(2), T. I. Toroshelidze(1), M. V. Vardosanidze(1), Q. M. Parade(1)

(1) Town Department of Abastumani Astrophysical Observatory of Georgian Academy of Sciences, A.Kazbegi av. 2a, 380060 Tbilisi, Georgia, E-mail: didebulidze@yahoo.com / didebulidze@posta.ge (2) Space Physics Research Laboratory, The University of Michigan, 2455 Hayward St., Ann Arbor, Michigan 48109-2143, U.S.A., E-mail: juliek@umich.edu

Abstract: Nightglow observations from Abastumani, Georgia (41.8 N, 42.8 E) are used to demonstrate sensitivity of the mesosphere-thermosphere regions to tectonic events. Enhancements in the nightglow intensity in the mid-latitude oxygen 557.7 nm green line (observed by L.M. Fishkova, 1983) are seen both preceding and following earthquakes (EQ) in the Caucasus region. Theoretical analysis suggests that the observed airglow perturbations are the result of strong changes in the thermospheric wind field accompanying an EQ event. Enhancements a few hours before the main EQ shock are considered as a possible result of an increase in the downward flux of oxygen atoms above this nightglow layer. In some cases the 557.7 nm line enhancement before an EQ is accompanied by a simultaneous decrease in the ionosphere F-region oxygen 630.0 nm red line intensity. These phenomena are considered to be caused by additional heating in the regions between the 95 km altitude of the 557.7 nm emission layer peak and the 240-300 km maximum in the 630.0 nm emission. Such a heating process is a possible source of both downward flux (for the 557.7 nm layer) and upward flux (for the 630.0 nm layer). Increases in the amplitude of short-period atmospheric gravity waves are also observed in both the 557.7 nm and 630.0 nm line nightglows during tectonic events. This increase in gravity wave activity is considered an important heating source due to molecular viscosity. Several cases of the regional effects in the 557.7 nm line intensity observed during strong tectonically disturbed days are shown.

3.2 GWV.02: SHORT-PERIOD ATMOSPHERIC GRAVITY WAVES AMPLITUDE AMPLIFICATION ON MAGNETICALLY DISTURBED DAYS AT THE MESOSPHERE-THERMOSPHERE HEIGHTS by Didebulidze, G.G.

Status of first author: non-student

Authors: G. G. Didebulidze(1), T. I. Toroshelidze(1), J. F. Kafkalidis(2), M. G. Shepherd(3), G. G. Shepherd(3), S. P. Zhang(3), M. V. Vardosanidze(1)

(1) Town Department of Abastumani Astrophysical Observatory of Georgian Academy of Sciences, A.Kazbegi av. 2a, 380060 Tbilisi, Georgia, E-mail: didebulidze@yahoo.com / didebulidze@posta.ge (2) Space Physics Research Laboratory, The University of Michigan, 2455 Hayward St., Ann Arbor, Michigan 48109-2143, U.S.A., E-mail: juliek@umich.edu (3) York University, Centre for Research in Earth and Space Science, 4700 Keele Str., Toronto, Ontario M3J 1P3, Canada, E-mail: gordon@windii.yorku.ca / mshepher@yorku.ca

Abstract: Strong amplification in the amplitude of short-period atmospheric gravity waves (AGWs) in the mesosphere-lower thermosphere (MLT) region on magnetically disturbed days is noted in the total nightglow intensity of the oxygen green line (557.7 nm) observed from Abastumani, Georgia (41.8 N, 42.8 E). This phenomena of increase in the MLT region short-period AGWs amplitude is more noticeable during spring and fall equinox days. On magnetically disturbed days close to equinox, in some cases the increase in green line intensity is accompanied by a simultaneous decrease in the ionospheric F region oxygen red line (630.0 nm)

intensity. This mutual correlation of the intensities of the MLT green line nightglow and the ionospheric F region red line nightglow is considered as a characteristic of the mesosphere-thermosphere-ionosphere coupling processes and the sensitivity of these regions to the temporal development of space weather. The horizontal wind field changes in the mid-latitude thermosphere on magnetically disturbed days is considered as an important mechanism responsible for the formation of the short-period and small scale AGWs in these regions.

3.3 GWV.03: Comparison of wind velocity between MU radar and FPI — – possible effect of OI5577 airglow height variation — by Fujii, Junsuke presented by Nakamura, Takuji

Status of first author: student not in poster competition Masters

Authors: Junsuke Fujii, RASC, Kyoto Univ. , fujii@kurasc.kyoto-u.ac.jp Takuji Nakamura, RASC, Kyoto Univ., nakamura@kurasc.kyoto-u.ac.jp Toshitaka Tsuda, RASC, Kyoto Univ., tsuda@kurasc.kyoto-u.ac.jp Kazuo Shikawa, STE lab., Nagoya Univ., shiokawa@stelab.nagoya-u.ac.jp

Abstract: We have compared wind velocities around mesopause height measured by meteor observation of the MU (Middle and Upper atmosphere) radar and OI (5577) airglow observation by FPI (Fabry-Perot Interferometer), at Shigaraki (34.8N), Japan, on November 13/14, 1999. When we assume the airglow height is constant throughout the night, it was difficult to find a single height exhibiting small r.m.s. difference between the two methods for both eastward and northward wind velocities. However, in case we introduce a time variation of airglow height due to a large scale gravity wave activity, we found very small r.m.s. wind difference by assuming the airglow height variation with an amplitude of 1.5 km, a period of 5.7 hours and a linear trend of -0.19 km/hour having the average height of 92.8 km. Further analysis of time and height variations of the wind and diffusion coefficient measured by the MU radar indicated that a gravity wave with a very similar structure predicted in the above comparison between the FPI and meteor winds has been detected as a dominant wave component. Thus, we suggest that the existence of gravity wave which can change the airglow height could lead the difference of wind velocities observed with FPI and radar techniques.

3.4 GWV.04: Height variation of OI5577 airglow observed by dual site all-sky imagers by Fukushima, Tetsuya presented by Nakamura, Takuji

Status of first author: student not in poster competition Masters

Authors: Tetsuya Fukushima, RASC, Kyoto Univ. , fuku@kurasc.kyoto-u.ac.jp Takuji Nakamura, RASC, Kyoto Univ., nakamura@kurasc.kyoto-u.ac.jp Yutaka Yamazaki, RASC, Kyoto Univ., yamazaki@kurasc.kyoto-u.ac.jp Toshitaka Tsuda, RASC, Kyoto Univ., tsuda@kurasc.kyoto-u.ac.jp Kazuo Shikawa, STE lab., Nagoya Univ., shiokawa@stelab.nagoya-u.ac.jp

Abstract: About one year observation of simultaneous dual-site all-sky imagers in Japan has been analyzed in order to derive OI5577 emission height. The analysis is based on the cross correlation of the two simultaneous images obtained at the different site (Kubota et al., 1999, Ejiri et al., 2002). We used band-pass filtered images with a pass band of 14-100 km horizontal wavelength, in order to extract freely propagation gravity waves, rather than instabilities in the airglow region. Significant day-to-day and periodic (2 - 6 hours) variation of the estimated heights could be recognized, which could be due to planetary waves and gravity waves, respectively. Clear annual variation of OI5577 height with August- September maximum (-98km) and February minimum (-93 km) was found.

3.5 GWV.05: Antarctic Observations on Hydroxyl Airglow. by French, John

Status of first author: non-student

Authors: W.J.R. French, University of Western Ontario/Australian Antarctic Division, jfrench@physics.uwo.ca R.P. Lowe, University of Western Ontario, lowe@physics.uwo.ca G.B. Burns, Australian Antarctic Division, gary.burns@aad.gov.au

Abstract: Night-time emissions from the hydroxyl layer over Davis station, Antarctica (68.6S, 78.0E) are monitored continuously by three ground based instruments.

A Czerny-Turner Spectrometer (CTS) has routinely scanned the OH(6-2) band since 1995 obtaining rotational temperatures. These have been used to characterize tidal, planetary scale, seasonal and solar cycle variations at Davis, and careful calibration has been maintained so that they may contribute to long-term trend studies.

More recently, a Fourier Transform Spectrometer (FTS) has been added to monitor several bands in the 1.5 micron region. This instrument incorporates a sun-tracking polaroid filter to allow observations to be extended into twilight, thus maximizing both diurnal and seasonal coverage of OH rotational temperature measurements.

In addition, a scanning radiometer (UWOSCR) installed in Jan-1999, scans a 16x16 degree field in the zenith each minute, to produce low resolution images of the hydroxyl layer. Characteristics of small scale gravity waves, propagating through the OH layer, can be deduced from these images. Methods of image sequence analysis and results are presented.

3.6 GWV.06: Simultaneous Mesospheric Wind, Gravity Wave and Temperature Measurements at Bear Lake Observatory, Utah (41.6 N) by Hatch, D.

Status of first author: student in poster competition Undergraduate

Authors: D. R. Hatch, M.J. Taylor, A. Taori(1) and W. Hocking (2), (1) Center for Atmospheric and Space Science, Utah State University, (2) Department of Physics, University of Western Ontario, Canada

Abstract: As part of a collaborative research program between the Space Dynamics Laboratory of Utah State University and the University of Western Ontario a meteor wind radar was installed and operated at Bear Lake Observatory, Utah (41.6 N, 111.6 W) alongside several instruments including a multi-wavelength all-sky imager and an OH/O₂ mesospheric temperature mapper (MTM). Joint measurements were obtained over a six month period during the winter from October 2000 to March 2001. The meteor radar data have been analyzed to determine the zonal and meridional winds at MLT heights (80-100 km) and to estimate the mesospheric temperature variability. The MTM data provide an independent measurement of mesospheric temperature for two emissions (OH and O₂) centered at about 87 and 94 km respectively. The all-sky image data have been investigated to quantify several prominent gravity wave events for the analysis of their intrinsic properties. This poster will focus on the comparison of the radar and imager results to date to help quantify mesospheric variability at mid-latitudes.

3.7 GWV.07: High Frequency Gravity Wave Damping in the Mesopause Region from Airglow Measurements at Albuquerque, New Mexico by Li, Feng

Status of first author: student not in poster competition PhD

Authors: Feng Li, Univ. of Illinois at Urbana-Champaign, fengli@uiuc.edu Alan Z. Liu, Univ. of Illinois at Urbana-Champaign, liuzr@uiuc.edu Gary R. Swenson, Univ. of Illinois at Urbana-Champaign, swenson1@uiuc.edu

Abstract: The OH Meinel band and the O₂ Atmospheric band (0,1) airglow were measured by an all-sky imager at Albuquerque, New Mexico (35 N, 106.5 W) between Nov. 1999 and May 2000. The simultaneous observations of the OH and O₂ airglow emissions make it possible to study the gravity wave dissipation in the mesopause region. Five quasi-monochromatic gravity wave events are analyzed. Amplitudes of the wave-induced airglow intensity perturbations in the OH and O₂ emission layers are extracted. The ratio of the amplitude in the O₂ airglow to that in the OH airglow is compared to a model prediction to estimate the wave damping rate. Our initial results show that the high frequency gravity waves are heavily damped in the mesopause region.

3.8 GWV.08: Low-Frequency Tropospheric Forcing as a Source of Quasi-Monochromatic Gravity Waves Observed in the Upper Mesosphere and Lower Thermosphere by Snively, Jonathan

Status of first author: student in poster competition Masters

Authors: Jonathan B. Snively, jbs231@psu.edu; Victor P. Pasko, vpasko@psu.edu; The Pennsylvania State University, Dept. of Electrical Engineering, CSSL.

Abstract: Airglow imaging reveals that quasi-monochromatic, small-scale, gravity waves frequently propagate through the upper mesosphere and lower thermosphere [Taylor et al., GRL, 22, 2849, 1995; Walterscheid et al., JASTP, 61, 461, 1999; Hecht et al., JGR, 106, 5181, 2001; and references cited therein]. It is widely believed that these observed waves may be guided or trapped by a thermal duct [e.g., Walterscheid et al., 1999]. Here we examine an oscillatory source in the troposphere associated with convection as a means to generate such observed quasi-monochromatic gravity waves. A new high-resolution, fully-compressible, two-dimensional model, which simulates the propagation of small-scale gravity waves in a realistic atmosphere, has been developed. The model is based on a flux-limited, high-resolution, finite volume method utilizing Randall LeVeque's CLAWPACK software package [LeVeque, J. Comp. Phys., 131, 327, 1997; <http://www.amath.washington.edu/claw>]. The model is able to identically satisfy an arbitrary steady-state atmosphere and can support solutions containing shocks or nonlinearities with minimal diffusion. This is necessary in the case of strong forcing, where nonlinear effects become significant. We consider a realistic thermal profile with ducts present in the stratosphere and lower thermosphere. A low-frequency oscillatory source is placed in the troposphere to produce a controlled spectrum of gravity waves. We first consider weak forcing, where radiated waves will remain linear through the simulation domain with a dominant forcing frequency too low to result in trapping or reflection. We then consider strong forcing, where nonlinear gravity wave breaking will occur at the altitude of the lower thermospheric duct. For this case, the source frequency remains unchanged, however higher order harmonics generated in breaking [Franke and Robinson, J. Atmos. Sci., 56, 3010, 1999] will be subject to some degree of trapping. We observe that nearly monochromatic waves, with wavenumber and frequency equal to twice that of the source, are consequently trapped in the lower thermospheric duct. This demonstrates that breaking waves may be a source of the enhanced spectrum necessary to populate the lower thermospheric duct [Vadas et al., J. Atmos. Sci., 60, 194, 2003]. We also explore coupling ("kissing") between the stratospheric and lower thermospheric ducts [e.g., Walterscheid et al., JGR, 106, 31825, 2001; and references cited therein] due to high frequency sources, which initially lead to trapping of waves in the stratospheric duct. Perturbation magnitudes, observed velocities, and spectral properties are discussed in detail and results are compared with observations, linear solutions, and analytical models.

3.9 GWV.09: Extraction of Gravity Wave Momentum Fluxes From Airglow Images by Tang, Jing

Status of first author: student in poster competition PhD

Authors: Jing Tang, Farzad Kamalabadi, Alan Z. Liu, and Gary R. Swenson Department of Electrical and Computer Engineering, University of Illinois at Urbana-Champaign
jingtang@uiuc.edu farzadk@uiuc.edu liuzr@uiuc.edu swenson1@uiuc.edu

Abstract: We propose a novel technique for calculating the vertical fluxes of horizontal momentum of high frequency gravity waves in the mesopause region with airglow images and meteor radar winds. This approach corrects the Doppler effect in a group of three consecutive images and generates two time differenced (TD) images. The two dimensional (2-D) cross periodogram of the two TD images are employed to identify the monochromatic wave components and to extract the wave parameters. In order to analyze the spatial disparity of the wave contents in addition to estimating the average parameters from the whole field of view (FOV), 2-D short-space Fourier transform is applied. With the wave parameters acquired, we calculate the momentum fluxes of the wave components in each TD image. The variation of the direction and strength of waves can be tracked for each clear night. Nightly averages provide information for investigating seasonal and geographical variations in momentum flux of gravity waves.

3.10 GWV.10: Five Minutes Gravity Waves due to Thunderstorm Activity in the Gulf of Mexico. by Martinez, Lisandro

Status of first author: student in poster competition Undergraduate

Authors: Lisandro M. Martinez Space Physics Research Lab. Embry Riddle Aeronautical University
martinel@sprl.db.erau.edu

Abstract: Short Period Gravity waves were found over the gulf of Mexico due to development of convective activity, which is produced by the instability of the atmosphere. To detect the short period waves, two Michelson Interferometers were used, one at Daytona Beach, FL, and the second one, placed in San Antonio, TX. Both instruments measure mesospheric temperatures at 80 Km. The instrument located at Daytona Beach looks over Tampa, and the one in San Antonio looks over Gainesville. Data was collected and analyzed for OH-31 and OH-42 temperatures. The derived temperatures were then analyzed using a Lomb-Scargle with a 10 minutes sliding window. Short period waves, with a period of 5 minutes were observed in the temperature data for Daytona Beach and San Antonio. It is hypothesized that these waves are generated as a result of convective activity produced during thunderstorms.

3.11 GWV.11: Airborne Investigations of Atmospheric Emissions (0.9 - 1.6 microns) using an InGaAs Camera by Nielsen, Kim

Status of first author: student not in poster competition PhD

Authors: K. Nielsen (1), M.J. Taylor (1), P. Jenniskens (2), D. Bushman (3), C. Miller (3), and R.A. Goldberg (4) (1) Center for Atmospheric and Space Science (CASS), Utah State University, (2) SETI Institute, NASA/Ames Research Center, (3) NASA/Dryden Flight Research Center, and (4) NASA/Goddard SFC

Abstract: Novel image measurements of OH mesospheric emissions and Leonid meteors were made using a sensitive Indium-Gallium-Arsenide (InGaAs) intensified camera during two NASA airborne campaigns; the Leonid MAC mission (November 2002), and the SOLVE II campaign (January 2003), using the NASA DC-8 Airborne Laboratory. For the Leonid mission three types of intensified cameras were operated, two narrow band imagers to investigate the ablation signatures of meteors, and an InGaAs imager to study gravity wave variability over a large range of longitudes (two trans-Atlantic flights). The SOLVE II airborne mission was based in Kiruna, Sweden, and several extended nighttime flights were made into the high arctic region to measure ozone concentrations in conjunction with the SAGE III satellite instrument. As part of this mission we were given the opportunity to extend our InGaAs measurement of mesospheric airglow wave structure and emissions to polar latitudes. This mission also coincided with the NASA MaCWave rocket campaign that was conducted from Esrange, Sweden during this period. In this poster we present initial results primarily of the InGaAs measurements, obtained during these two missions.

3.12 GWV.12: Equatorial MLT Gravity Wave Measurements by Olsen, Christian

Status of first author: student in poster competition Undergraduate

Authors: Olsen, C. L., Taylor, M. J., Center for Atmospheric and Space Sciences, Utah State University
Vincent, R. A., Department of Physics, University of Adelaide, Australia

Abstract: During the fall of 1995, a USU all-sky airglow imager was operated from Christmas Island, Republic of Kiribati (2.00 N, 157.50 W), in conjunction with long-term MF radar wind measurements. Image measurements of the Na, OI (557.7 nm), and near infrared OH band emissions were obtained during the period of 14 September-2 October. A total of 45 extensive, short-period, gravity wave events were extracted from the multi-wavelength images and their intrinsic wave properties were determined using the background mesospheric wind data. The MLT zonal wind during this period was predominately westward, while the majority of the gravity waves ($\approx 80\%$) exhibited an eastward component of propagation. These measurements

will be compared and contrasted with wave data from several sites at other latitudes. Estimates of the momentum fluxes associated with these wave events will also be presented together with a discussion of the uncertainties in these results.

3.13 GWV.13: Multi-Diagnostic Measurements of a Large Gravity Wave Event at Arecibo Observatory, Puerto Rico. by Smith, Steve

Status of first author: non-student

Authors: Steve M. Smith, Boston University. smsm@bu.edu Jonathan Friedman, Arecibo Observatory. jonathan@naic.edu Shikha Raizada, Arecibo Observatory. shikha@naic.edu Craig Tepley, Arecibo Observatory. craig@niac.edu Rob Wilson, Arecibo Observatory. rob@niac.edu Jeffrey Baumgardner, Boston University. jeff@bu-ast.bu.edu Michael Mendillo, Boston University. mjmendillo@aol.com

Abstract: A large bore-like gravity wave event was observed by the Boston University all-sky imager at Arecibo Observatory in several mesospheric airglow emissions (557.7nm, 589.3nm and OH in the near infrared) during the night of 2/3 May 2003. Simultaneous measurements of the 70 to 120 km height region, made by two co-located lidars, indicated that a large temperature increase occurred at the time of the event's onset. The observations, analysis and interpretation of the event are discussed.

3.14 GWV.14: GRAVITY WAVE PROPAGATION MEASURED IN BRAZILIAN EQUATORIAL AND MIDDLE LATITUDE REGION by Wrasse, Cristiano

Status of first author: student not in poster competition PhD

Authors: Wrasse, C.M.(1), Nakamura, T.(2), Takahashi, H.(1), Medeiros, A.F.(4), Buriti, R. A(4), Taylor, M.J.(3), Gobbi, D.(1)

1-Instituto Nacional de Pesquisas Espaciais, INPE, Brazil - 2-Radio Science Center for Space and Atmospheric, RASC, Kyoto University, Kyoto, Japan 3-Universidade Federal de Campina Grande, UFCG, Campina Grande, PB, Brazil 4-Space Dynamics Laboratory and Physics Department, Utah State University, Logan, Utah, USA

Abstract: Recently, airglow imaging observations in the mesopause region have been carried out at many places using CCD imagers. This technique provides useful information about the gravity wave horizontal structure, wavelength, phase velocity and period. In this work we present characteristics of the atmospheric gravity waves observed at S. J. Cariri (7 S, 36 W) and Cachoeira Paulista (22.7S, 45 W), Brazil. A ray tracing technique was also applied in the imaging data in order to find out the gravity wave sources and to investigate the propagation of these waves through the atmosphere. The CIRA-86 reference zonal wind and temperature models and the GSWM-02 tidal wind model were used as the background condition in the present analysis. We investigate the tidal wind effects on the gravity wave propagation through the middle atmosphere and find out the source region and the possible generation mechanism.

3.15 GWV.15: Characteristics of inertio-gravity waves in the upper troposphere and lower stratosphere over the South Pacific as revealed by GPS radiosondes by Yamamori, Miho

Status of first author: non-student

Authors: Miho Yamamori (Communications Research Laboratory, Japan, yamamori@crl.go.jp) Kaoru Sato (National Institute of Polar Research, Japan, kaoru@nipr.ac.jp)

Abstract: A cruise experiment MeSSO2001 (a Meridional Scan of the Stratosphere over the Ocean in 2001) was performed in order to know the characteristics of small-scale atmospheric disturbances over the ocean (Sato et al., 2003). During about one month of December 2001, Vaisala RS-15GH radiosondes were launched

at almost the same latitude interval of 1 degree in the latitude range of 28 N to 48 S over the middle Pacific from a research vessel.

By using the horizontal wind and temperature data with fine vertical resolution, we investigated characteristics of inertio-gravity waves in the upper troposphere and lower troposphere in the sub- and extra-tropics over the South Pacific where very few radiosonde observations have been made. Wave parameters were estimated by hodograph analysis together with the dispersion relation. It was found that dominant direction of horizontal propagation was southward, with a little bias toward southeastward. A notable northward propagation of gravity waves was found in the sub-tropical lower stratosphere. The source of the gravity waves was estimated as a cutoff cyclone developing in the upper troposphere through ray tracing analysis.

3.16 GWV.16: A Full-Wave Investigation of the Use of a 'Cancellation Factor' in GW-Airglow Interaction Studies by Yu, Yonghui

Status of first author: student in poster competition Masters

Authors: Yonghui Yu Department of Physical Sciences Embry-Riddle Aeronautical University
 yu_yonghui@yahoo.com
 Michael P. Hickey Department of Physical Sciences Embry-Riddle Aeronautical University
 Michael.Hickey@erau.edu

Abstract: Atmospheric gravity waves (GWs) perturb minor species involved in the chemical reactions of airglow emissions in the upper mesosphere and lower thermosphere. Numerical modeling has previously shown that the airglow relative brightness fluctuation can be much larger than the brightness-weighted relative temperature fluctuation (that is, Krassovsky's ratio is much greater than 1). In order to determine wave fluxes and the forcing effects of gravity waves on the mean state, it is most useful to be able to correlate the airglow brightness fluctuation amplitude to the major gas density fluctuation amplitude. This can be performed through modeling, but Swenson and Gardner (and later Swenson and Liu) derived analytic expressions relating the two through a so-called 'cancellation factor' (CF). Certain approximations were made by them in deriving the CF. The validity of these approximations and the accuracy of the derived CF are investigated here using a full-wave model describing gravity wave propagation in a non-isothermal, windy, and viscous atmosphere. The full-wave model (combined with a five-reaction photochemical scheme) is used to derive fluctuations in the OH nightglow from which an equivalent CF is calculated. Extensive comparisons between our CF and that of Swenson and colleagues show under what atmospheric conditions and range of wave parameters the Swenson and colleagues CF would be expected to provide a good measure of GW density fluctuation amplitude using airglow observations. It is important that GW amplitude be determined as accurately as possible because wave fluxes are proportional to the square of wave amplitude.

4 Tuesday Evening 17 June 2003 Poster Session Abstracts, Other waves (tidal, planetary, small scale, etc.)

4.1 OWV.01: Variability in the mesosphere and ionosphere during the April 2002 by Goncharenko, Larisa

Status of first author: non-student

Authors: Goncharenko L., MIT Haystack Observatory, R. Clark, University of New Hampshire, I. Galkin, University of Massachusetts Lowell, G. Khmyrov, University of Massachusetts Lowell, A. Manson, University of Saskatchewan, Canada, C. Meek, University of Saskatchewan, Canada, N. Mitchell, University of Bath, UK, Y. Murayama, Communications Research Lab., Japan, R. Niciejewski, University of Michigan, D. Riggin, Colorado Research Assoc., J. Salah, MIT Haystack Observatory, W. Singer, Rostock University, Germany, Q. Wu, National Center for Atmospheric Research, S. Zhang, York University, Canada

Abstract: We investigate the structure of the global mesosphere and ionosphere using multi-instrument observations during the April 2002 period, with focus on geomagnetically quiet periods. The observations from the array of MF and meteor radars show global presence of planetary wave disturbances, with periods ranging from 3-4 to 14 days. These oscillations are most pronounced in the zonal wind at high and middle latitudes, and subside at lower latitudes. We present preliminary results of search for similar variations in winds from the TIDI instrument on board of TIMED spacecraft.

Analysis of F-region ionospheric data from the network of ionosondes shows evidence of planetary scale variations in both electron density and the height of the F-layer. As these variations can not be accounted for by changes in geomagnetic activity and solar flux, we examine the possibility of influence of the planetary wave originating in the middle atmosphere on the thermosphere-ionosphere system.

4.2 OWV.02: Small-Scale Wave Structures in OH Airglow and Simultaneous Na Lidar Instability Observations by Li, Tao

Status of first author: student in poster competition PhD

Authors: Tao Li, Colorado State University, taoli@lamar.colostate.edu B. P. Williams, Colorado State University, biffw@lamar.colostate.edu T. Yuan, Colorado State University, titus@lamar.colostate.edu K. Arnold, Colorado State University, arnold@lamar.colostate.edu C. Y. She, Colorado State University, joeshe@lamar.colostate.edu D. A. Krueger, Colorado State University, krueger@lamar.colostate.edu

Abstract: The Platteville OH imager has observed the nighttime all sky images of OH (875km) airglow layers since September 2001. Here we will present our observations of small-scale wave structures (5 to 15km horizontal wavelength with lifetimes of less than 45min), also called ripple-type wave structures [Taylor and Hapgood, 1990; Hecht et al., 1997; Fritts et al., 1997], and the results of comparison with the derived atmospheric convective and dynamical instability from the nearby simultaneous CSU Na Lidar observations of temperature, zonal wind, and meridional wind. We found that the small-scale wave structures appear at almost same time with the local instability and also both have the same lifetime scale. Therefore we believe these small-scale wave structures are associated with the localized instability and wave breaking. It is also noted that these small-scale wave fronts are perpendicular to the fronts of main waves (30 to 50km horizontal wavelength) and the small-scale wave packages move opposite to the propagation direction of main waves.

4.3 OWV.03: Interannual and subseasonal variability of diurnal tides and tropospheric diurnal heating by Lieberman, Ruth

Status of first author: non-student

Authors: Ruth S. Lieberman and Dennis Riggin Northwest Research Associates Colorado Research Associates Division 3380 Mitchell Lane Boulder, CO 80301
ruth@co-ra.com

Abstract: We present analyses of tropospheric diurnal heating, and middle atmosphere diurnal tides. Our study highlights sub-seasonal and interannual variations, which have received comparatively little attention in the literature. Analysis of 12 years of data from the Kauai MF radar reveals significant interannual amplitude enhancements in the diurnal tide, particularly during 1992 and 1997. The amplitude maximum in 1997 is correlated with above-average tropical tidal heating due to IR absorption by water vapor. Examination of 10 years of monthly averaged tropospheric diurnal water vapor heating reveals an interannual component that maximizes over the Indian and tropical central Pacific oceans. This component explains over 40% of the total variance in the 10-year diurnal water vapor heating. We also explore the role of convective heating in modulating tropospheric diurnal forcing interannually.

Subseasonal (25–90-day) variability is also detected in Kauai diurnal winds, and in diurnal water vapor heating in the Indian and tropical Pacific Ocean. Previous studies have hypothesized that the tropospheric Madden-Julian, or intraseasonal oscillation can modulate tidal forcing. It has also been suggested that migrating tide and planetary wave interactions can modulate tidal amplitudes in the middle atmosphere on a week-to-week basis. Possible examples of this phenomenon are shown using LIMS temperatures during November 1978–May 1979.

4.4 OWV.04: Quasi-two-day variations observed by airglow and meteor wind in the equatorial region by Lima, Lourivaldo Mota

Status of first author: student not in poster competition PhD

Authors: Lourivaldo Mota Lima, INPE/UEPB, lourival@laser.inpe.br Hisao Takahashi, INPE, hisao@laser.inpe.br Paulo Prado Batista, INPE, pbatista@laser.inpe.br Delano Gobbi, INPE, delano@laser.inpe.br Ricardo A. Buriti, UFCG, rburiti@df.ufpb.br Takuji Nakamura, RASC-Kyoto University, nakamura@kurasc.kyoto-u.ac.jp Toshitaka Tsuda, RASC-Kyoto University, tsuda@kurasc.kyoto-u.ac.jp

Abstract: Simultaneous airglow emission observations at Sco Joco do Cariri (7:5, 35: W), Brazil and meteor winds at Jakarta (6.4: S, 106.7: E), Indonesia, were used to study the quasi-two-day periodic oscillations. In the present work, attention was given to the quasi-two-day wave event observed during July 05-16, 1999. The amplitude oscillation of the quasi-two-day variations of the airglow intensities were found to be 25% for OI5577 green line, 21% for O2 atmospheric band and 10% for OH (6-2) Meinel band. During the same period the meridional wind showed strong quasi-two-day oscillations with amplitude varying with height reaching a maximum value of about 21 m/s. The phase variation with height showed that the time of the maximum meridional winds took place earlier at greater heights, indicating descending phase and therefore an upward energy propagation. The present results suggest that the quasi-two-day variability observed in the airglow intensities should have the same origin as that of the wind oscillation, which is the quasi-two-day planetary wave.

4.5 OWV.05: Impact of Lower Atmosphere Forcing on Electrodynamical Variability in the Equatorial Ionosphere and Thermosphere by Maruyama, Naomi

Status of first author: non-student

Authors: N. Maruyama (1), T. J. Fuller-Rowell (Tim.Fuller-rowell@noaa.gov)(1), M. Codrescu (Mihail.Codrescu@noaa.gov)(1), A. Richmond (richmond@hao.ucar.edu) (2), R. Garcia (rgarcia@ucar.edu) (3) and G. Millward (george@apl.ucl.ac.uk) (4) (1) NOAA, Space Environment Center, (2) NCAR, High Altitude Observatory, (3) NCAR, Atmospheric Chemistry Division, (4) Atmospheric Physics Lab., University College, London

Abstract: Understanding the day-to-day variability in low-latitude electric fields and currents has been an important issue in the low-latitude ionosphere and thermosphere. The quiet-time equatorial vertical plasma (EB) drifts depend upon the relative importance between E- and F-region ionospheric dynamo processes, which require the field-line-integrated winds and electrical conductivities, and therefore require

understanding the coupling between lower and upper atmospheres. Possible sources of the quiet-time day-to-day variability in the electrodynamics can arise from changes in the global wind system and their resultant dynamo conditions, and changes in conductivity due to solar flux variability. The fluctuations in the wind can result from day-to-day and hour-to-hour changes in either the geomagnetic forcing at high latitudes or tidal/wave forcing from the lower atmosphere. CTIP, a model of coupled thermosphere, ionosphere, plasmasphere, with self-consistent electrodynamics, will be utilized in order to evaluate the impact of the sources of variability on the global electric fields and currents, and the resultant plasma drifts. Realistic changes in the propagating tidal wind and wave sources from the lower atmosphere will be simulated by using results from the Whole Atmosphere Community Climate Model (WACCM). Furthermore, the relative importance of the proposed different sources of variability will be addressed.

4.6 OWV.06: Investigations of the 8-hr wave in the mesosphere and thermosphere by Mutiso, Charles

Status of first author: student in poster competition Undergraduate

Authors: Charles Mutiso Embry-Riddle Aeronautical University 600 S. Clyde Morris Blvd Daytona Beach, Fl 32114 mutisoc@erau.edu

Abstract: Optical measurements of mesospheric temperatures will be analyzed to investigate the possible origins of the 8-hr wave. Two sets of continuous temperature data will be employed: a 5 month time-series from a Michelson Interferometer located at the South Pole and a 6 month time-series from a CCD Spectrometer at Sondrestromfjord, Greenland. The data will be analyzed to estimate the short term variability in the 8-hr wave and to investigate the non-linear contributions of the 12-hr and the 24-hr waves as a possible generation mode for the 8-hr wave.

4.7 OWV.07: Identifying tides and planetary waves in night-time LIDAR data using the Lomb-Scargle periodogram by Nelson, Karen

Status of first author: student in poster competition Masters

Authors: Nelson, Karen L. M., USU/CASS, slh5l@cc.usu.edu Wickwar, Vincent B., USU/CASS, wickwar@aeronomy.cass.usu.edu

Abstract: Tides and planetary waves play an important role in the dynamics of the middle atmosphere. There are inherent difficulties in identifying these oscillations in data that lack either day-time or night-time observations or have gaps in the sampling due to other difficulties (weather, instrumentation, observation windows, etc.). The Lomb-Scargle periodogram is an alternative to traditional Fourier analysis that resolves the problem of gaps in data. Here, the procedure is described and applied to night-time only Rayleigh LIDAR data.

4.8 OWV.08: Mean wind and atmospheric tide observed at Tromsø and Poker Flat by Nozawa, Satonori

Status of first author: non-student

Authors: S. Nozawa, Nagoya University, nozawa@stelab.nagoya-u.ac.jp H. Iwahashi, Nagoya University, iwahashi@stelab.nagoya-u.ac.jp S. Oyama, University of Alaska, soyama@gi.alaska.edu Y. Murayama, CRL, murayama@crl.go.jp A. Brekke, University of Tromsø, Asgeir.Brekke@phys.uit.no C. M. Hall, University of Tromsø, chris.hall@phys.uit.no A. Manson, University of Saskatchewan, manson@skisas.usask.ca C. Meek, University of Saskatchewan, meek@dansas.usask.ca R. Fujii, Nagoya University, rfujii@stelab.nagoya-u.ac.jp

Abstract: In order to understand the atmospheric dynamics in the polar mesosphere/lower thermosphere more deeply, we have investigated mean winds as well as atmospheric waves such as planetary, tidal and gravity waves based on wind data obtained with MF radars, meteor radars and EISCAT radars. In this talk,

based on MF radar wind data obtained at Tromsø (69.58 deg N, 19.22 deg E) and Poker Flat (65.1 deg N, 147.5 deg W), we report characteristics of mean wind as well diurnal and semidiurnal amplitudes and phases in the polar mesosphere between 70 and 91 km. At now, we have analyzed wind data from November 1998 to January 2003. We averaged wind data according to time and altitude, and made a 1-month averaged wind data as a function of time and altitude. Then, we derived mean wind velocities as well as diurnal and semidiurnal amplitudes and phases. Results are summarized as follows: (1) Mean wind. (a) Similar variations in time are found over the 4 years. (b) Between 82 and 91 km, at Tromsø a semiannual variation is found: the meridional mean wind blows southward with an amplitude of 10 m/s in summer and winter, while it blows northward or close to 0 in spring and fall. At Poker Flat in the same altitude region, the meridional mean wind blows southward in summer as well, but it is northward from fall to spring. (c) At and below 85 km, the zonal mean wind exhibits an annual variation: it blows westward with its maximum amplitude 30-40 m/s in summer and eastward with its maximum about 20 m/s in winter. The westward wind amplitude is stronger by about 10 m/s at Poker Flat than at Tromsø. (2) Diurnal tide. (a) The diurnal amplitude exhibits a similar annual variation over the four years. (b) At Tromsø at and above 79 km, the amplitude is stronger (10-15 m/s) in summer and weaker (about 5 m/s) in winter. (c) At Poker Flat, the amplitude does not exhibit a clear seasonal variation, but it is about 5-10 m/s through a year. (d) The corresponding phase values of the meridional component, where the phase stands for a local time of northward maximum, are about 12 LT through a year, and a year-to-year variation of the phase is not significant. (e) For phase values of the zonal component, where the phase stands for local time of eastward maximum, their variation in time is less significant as well. (3) Semidiurnal tide. (a) The amplitude tends to increase with altitude increasing, and it is about 5 m/s at 70 km and about 15-20 m/s at 91 km. (b) At Tromsø, the amplitude maximizes in September over the 4 years, and also it becomes stronger in January and February. (c) At Poker Flat, the amplitude does not vary in time significantly except for April when its amplitude is the weakest through a year over the 4 years. (d) At Tromsø, phase values exhibit a similar variation in time over the 4 years and the difference of year-to-year values are less than 3 hours. (e) At Poker Flat, a similar tendency with that of Tromsø is found, but it varies largely in April.

4.9 OWV.09: INVESTIGATING MESOSPHERIC OH AND O2 TEMPERATURE VARIABILITY AT LOWLATITUDES OVER MAUI, HAWAII. by Taori, A

Status of first author: non-student

Authors: A. Taori, M. J. Taylor and D. Hatch Center for Atmospheric and Space Science, Utah State University, USA. alok@cc.usu.edu,mtaylor@cc.usu.edu,drhatch@cc.usu.edu

Abstract: The USU-CEDAR Mesospheric Temperature Mapper (MTM) has been operated from Maui, Haleakala (20.8N, 156.2W) since October 2001, as a part of the Maui-MALT campaign. The MTM measures OH (6,2) and O₂ (0,1) Atmospheric band intensities using a narrow band (1 nm FWHM) interference filters. The OH and O₂ rotational temperatures are deduced with a precision of 1-2 K in 6 minutes. Over 18 months of quality data have been obtained to date, permitting a novel study of the mesospheric temperature variability over two altitude regions centered on 87 and 94 km. These include, seasonal variation, monthly averaged nocturnal variation (large amplitude tide-like structures), inter-annual comparison of monthly mean temperature variations and possible planetary wave signatures. In this poster we present initial results of these studies of mesospheric temperature variability at low-latitudes.

4.10 OWV.10: Yearlong Na-Lidar observation of temperature and winds over full diurnal cycles above Ft. Collins, CO (40N, 105W) by Yuan, Tao

Status of first author: student in poster competition PhD

Authors: Tao Yuan – Physics Department, Colorado State University titus@lamar.colostate.edu Kam Arnold -Physics Department, Colorado State University arnold@lamar.colostate.edu B. Williams - Physics Department, Colorado State University biffw@lamar.colostate.edu C.Y.She – Physics Department,

Colorado State University joeshe@lamar.colostate.edu D.Krueger –Physics Department, Colorado State University krueger@lamar.colostate.edu Maura Hagan-NCAR, hagan@hao.ucar.edu

Abstract: With a pair of robust Faraday Filters, Na-Lidar in Colorado State University has observed mesopause region temperature and winds (80-110km) over full diurnal cycle for one year. Here, we select only continuous 24-hour data sets for analysis. We observed considerable daytime and nighttime differences for both temperature and winds (Zonal and Meridional). We investigated the tidal wave (Diurnal and Semi-Diurnal) activities and compared with GSWM (Global Scale Wave Model). Observed diurnal tides are in good agreement with GSWM prediction, though some discrepancies exist in semidiurnal tides comparison. Larger amplitude and shorter wavelength than what model predict are typically observed for semidiurnal tides.

4.11 OWV.11: Interpretation of apparent storm-related effects in the mesosphere at high latitudes during April 2002. by Zhang, Shengpan

Status of first author: non-student

Authors: Shengpan Zhang, MIT Haystack Observatory, sheng@stpl.cress.yorku.ca R. Clark, University of new Hampshire, ron.clark@unh.edu L. Goncharenko, MIT Haystack Observatory, lpg@haystack.mit.edu M. Hagan, HAO NCAR, hagan@hao.ucar.edu G. Lu, HAO NCAR, ganglu@hao.ucar.edu N. Mitchell, University of Wales, UK, N.J.Mitchell@bath.ac.uk R. Niciejewski, University of Michigan, niciejew@umich.edu Q. Wu, HAO NCAR, qwu@hao.ucar.edu J. Oberheide, HAO NCAR, jenso@ucar.edu Y. Murayama, Communications Research Lab. Japan, murayama@crl.go.jp R. Roble, HAO NCAR, roble@hao.ucar.edu J. Salah, MIT Haystack Observatory, jes@haystack.mit.edu W. Singer, Leibniz-Institute of Atm. Phy, Germany, singer@iap-kborn.de J. Thayer, SRI, j.thayer@sri.com A. van Eyken, EISCAT, Tony.van.Eyken@eiscat.com

Abstract: During the April 2002 geomagnetic storm, two MLT radars at Andenes (69N) and Esrange (68N) reveal wind patterns at mesospheric altitudes that appear to be similar to the expected ion convection pattern at these latitudes. The pattern seen at the peak of the storm on April 17 is not seen on other quiet or disturbed days at these two locations, or at other locations. It may be possible that the winds in the mesosphere are a manifestation of a localized effect in the sunlit sector. Correlations with plasma variations in the ionosphere from incoherent scatter radars at high latitudes have been sought, but are inconclusive. TIDI winds in April 2002 are also examined for a potential response to the storm effects. Preliminary simulations of TIME-GCM/AMIE for the storm have been developed at NCAR, and comparisons with the observations are made to determine whether the observed effects are induced by the storm. The interpretation of the storm effects is particularly challenging due to the presence of large planetary waves that are observed prior to the beginning of the storm.

4.12 OWV.12: Seasonal, annual, and long-term airglow emission rate variabilities in the mesosphere and lower thermosphere observed by WINDII during 1990's by Zhang, Shengpan

Status of first author: non-student

Authors: Shengpan Zhang, MIT Haystack Observatory/York University Canada, sheng@stpl.cress.yorku.ca Gordon G. Shepherd, York University, Canada, gordon@YorkU.CA

Abstract: Airglow volume emission rate measurements by WINDII on UARS during 1990's provide a vast amount of scientific data in a global scale for studying seasonal, annual, and long term variabilities of the airglow, and their dependence on chemistry, dynamics, solar radiation, and possibly trace gases from human activity. The main features of WINDII airglow measurements are (1) annual variations (summer maximum) in dayglow and semiannual variations (equinoctial maxima) in nightglows at high and mid-latitudes, (2) equatorial minimum and maximum in O(1S) and OH nightglows, respectively, due to diurnal tides, (3) strong correlations of Solar 10.7cm flux with daytime O(1S) and O(1D) emissions at low latitudes but a weak correlation with the daytime O2 band emission.

4.13 OWV.13: Nonmigrating Tides as Measured by the SABER Instrument on TIMED during April, 2002: The Aliasing Problem by Zhang, Xiaoli

Status of first author: student in poster competition

Authors: Xiaoli Zhang, Scott E. Palo and Jeffrey M. Forbes

Department of Aerospace Engineering Sciences UBC 429, University of Colorado, Boulder, CO 80309-0429.
(e-mails: xiaoli.zhang@colorado.edu, scott.palo@colorado.edu, jeffrey.forbes@colorado.edu)

Abstract: Temperature measurements from the SABER instrument on TIMED are used to investigate migrating and nonmigrating solar tides from -82 to $+51$ degrees latitude between about 50 and 100 km altitude during April, 2002. The most prominent nonmigrating tide oscillations include eastward-propagating diurnal tides near the equator and tropics, and semidiurnal tides with zonal wavenumbers $s = 1$ and $s = 3$ at higher latitudes. However, there are indications that some of these tidal signals may include aliasing contributions from other tides or/and background variation (i.e. terdiurnal tides or/and 30-day oscillation). In this poster, we will address the aliasing problems in analysing satellite-based measurements like SABER data.

5 Tuesday Evening 17 June 2003 Poster Session Abstracts, Instruments and techniques for middle atmospheric and ionosonde observations

5.1 IMI.01: The SHIMMER Instruments: Spatial Heterodyne Imagers for Remote Sensing of the Atmosphere from Space by Englert, Christoph R.

Status of first author: non-student

Authors: Christoph R. Englert Naval Research Laboratory Code 7641 4555 Overlook Ave. SW Washington, DC, 20375 USA Christoph.Englert@nrl.navy.mil
 Joel G. Cardon Naval Research Laboratory Washington, DC, USA cardon@uap2.nrl.navy.mil
 John M. Harlander St. Cloud State University, Minnesota, USA harlander@stcloudstate.edu
 Fred L. Roesler University of Wisconsin - Madison, Wisconsin, USA roesler@wisp.physics.wisc.edu
 Michael H. Stevens (Naval Research Laboratory) Naval Research Laboratory Washington, DC, USA stevens@uap2.nrl.navy.mil

Abstract: The NRL-SHIMMER (Spatial Heterodyne Imager for MEsospheric Radicals) program was initiated about a decade ago in collaboration with the University of Wisconsin and St. Cloud State University with the goal to provide long term, global measurements of OH in the middle atmosphere using high resolution UV remote sensing. Our recent advances in Spatial Heterodyne Spectroscopy (SHS) allow us to design and build much smaller, lightweight, and rugged instruments that will outperform their predecessor experiment MAHRSI (Middle Atmosphere High Resolution Spectrograph Investigation) which utilized conventional grating spectroscopy. The SHS technique is similar to a Michelson spectrometer or FTS, with the retro-reflectors in the interferometer arms replaced by fixed, tilted gratings at equal distance from the beamsplitter. Diffraction on the gratings results in a wavenumber dependent tilt of the recombining wavefronts, creating Fizeau fringes that are detected with a position sensitive detector (CCD). Field widened SHS instruments designed for measuring OH around 308 nm are the core of the SHIMMER program, which currently consists of two flight projects: SHIMMER-Middeck and SHIMMER-STPSat-1. Like MAHRSI, the SHIMMER instruments observe the sunlit limb from low earth orbit using a narrow bandpass around 308 nm. The imaging capability of SHS is used to observe the limb between about 30 km and 100 km so that no scanning mirror is required. We present data from the proof of concept flight of SHIMMER on the Space Shuttle in October 2002 and a status report on the STPSat-1 instrument including first laboratory measurements performed with a monolithic SHS interferometer.

5.2 IMI.02: A Stereoscopic imaging method for measuring the altitude of the near infrared airglow layer by Faivre, Michael

Status of first author: student in poster competition PhD

Authors: M. Faivre (1) michael.faivre@obs-besancon.fr
 G. Moreels (1) moreels@obs-besancon.fr
 D. Pautet (2) pautet@cc.usu.edu
 J. Clairemidi (1)
 F. Colas (3)

(1) Observatoire de Besancon, 25010, France (2)Center for Atmospheric Space and Science and Physics Department, Utah Sate University (3) Institut de Mcanique Cleste, 77 Ave.Denfert-Rochereau, 75014 Paris, France

Abstract: A program for determining the altitude of the barycenter of the near-infrared emissive layer at the mesopause level has been undertaken. The objective is to measure the two geometric parameters of the emissive layer: its altitude and thickness in order to correlate these values with the parameters of the dynamic processes that propagate at those altitudes. A first set of correlated observations was obtained in september 2000. Two cameras were set in simultaneous operation at Pic du Midi Observatory (Hautes-Pyrnes, altitude

2860 m) and at Pic de Chteau-Renard (Hautes-Alpes, altitude 2989 m). The azimuths of the lines of sight were opposite along the line that joined the two observation points. The star images were removed using a numerical filter. Then the perspective inversion method developed by Pautet (Applied Optics 41, 823-831, 2002) was used to provide images of the emissive layer as seen by a virtual camera located vertically above the observation sites. The intensity normalized cross correlation coefficient is computed for matched pixel blocks. The results for the night of September 8-9, 2000 will be presented. In the region where the fields of view of the cameras superimpose, the altitude for the maximum of the airglow intensity is 87.3 km. This value is the mean value for the altitude determinations performed within several square regions of interest. The median value is the same: 87.3 km. The emissive layer profile is retrieved with a height resolution of 0.2 km. The layer is located between the extreme altitudes of 85.4 and 89.9 km. A 2D chart representing the altitude of the layer barycenter is compared with a 2D representation of the emission intensity. In conclusion, a precise method for retrieving the near-IR airglow layer altitude with a precision of 0.2 km has been developed and will be used for measuring the altitude of the layer barycenter at different points of the wave field.

5.3 IMI.03: Microcontroller-Based Closed-Loop Laser Tuning System by Peshave, Manasi

Status of first author: student in poster competition Masters

Authors: Manasi Peshave University of Alaska Fairbanks ftmap@uaf.edu
Richard Collins University of Alaska Fairbanks rlc@gi.alaska.edu

Abstract: This poster presents the design of a closed-loop microcontroller based laser tuning system. The goal is to precisely control the tuning of a dye laser at Poker Flat Research Range (PFRR). This laser is used as a transmitter in a resonance lidar system. During operation, the operating frequency of the laser changes due to the change in the properties of the air inside the laser cavity.

A Motorola 68HC12A4 microcontroller is used in the closed-loop system. One tenth of the light leaving the laser is fed to the sodium Hollow Cathode Tube (HCT) sensor. The magnitude of the signal from the HCT is a sensitive function of the wavelength of the light incident on the HCT. This signal is processed with analog circuitry and is then fed to the microcontroller. The microcontroller then controls the laser tuning by changing the pitch of the laser diffraction grating.

5.4 IMI.04: Application Of The Ucar-stars Method To MF Radars by Praskovskaya, Eleanor

Status of first author: non-student

Authors: Eleanor Praskovskaya, Colorado Research Associates, epraskov@ucar.edu Alexander Praskovsky, NCAR, praskov@ucar.edu Dennis Riggin, Colorado Research Associates, Riggin@colorado-research.com Werner Singer, Leibniz-Institute of Atmospheric Physics, Germany, singer@iap-kborn.de

Abstract: UCAR-STARs is a new data processing technique for spaced antenna profiling radars. The abbreviation stands for the "University Corporation for Atmospheric Research - Structure function Analysis of Received Signals". STARs is based on analysing the different order cross and auto structure functions of the received signal's power for retrieving the mean horizontal velocity components and turbulence characteristics of a scattering medium. Overview of the UCAR-STARs method is presented, and the major steps of the data analysis technique are illustrated. Examples of wind measurements with Mesosphere-Stratosphere-Troposphere (MST) radars such as the Middle and Upper Atmosphere radar (MU), in Japan, and the Chung-Li, in Taiwan, Republic of China are presented. The major focus of the paper is on the Saura MF radar in Norway. Measurements of the mean horizontal wind speed components and turbulence intensity at height from 50 km to 100 km with temporal resolution 2 min. are presented and discussed. Propagation of atmospheric waves both in horizontal and vertical directions is demonstrated. Whenever is possible, the STARs retrieved mean horizontal wind speed components are compared with those by FCA and DBS methods as well as meteor scatter radars.

5.5 IMI.05: The structure function-based approach to data analysis for spaced antenna radars: a comparison with traditional techniques by Praskovsky, Alexander

Status of first author: non-student

Authors: Alexander Praskovsky, NCAR, praskov@ucar.edu Eleanor Praskovskaya, Colorado Research Associates, epraskov@ucar.edu

Abstract: Traditional methods of data analysis for spaced antenna (SA) radars deploy cross and auto correlation functions (CF) and spectra (SP) of multiple received signals for retrieving the mean velocity components, turbulence intensity, and other characteristics of a scattering medium. Cross and auto structure functions (SF) represent an alternative tool for such an analysis. The major advantage of the SF-based approach with respect to the CF and SP-based approaches is that SF of received signals can be derived and applied to practical measurements for any order equal, or larger than 2; the higher-order SF provide supplemental information about a scattering medium. On the contrary, only the second order CF have been used in SA methods, and SP are the second order functions as well. Other advantages of the SF-based approach are the following. * Relations between parameters of SF and characteristics of the diffraction pattern and a scattering medium can be derived with a smaller number of less restrictive assumptions than the corresponding relation for CF and SP. More universal and asymptotically exact equations for SF provide a deeper insight and more rigorous theoretical background for SA methods. * Turbulence characteristics can be related to the SF parameters more rigorously than to parameters of CF and SP. Moreover, the intensity of all three turbulent velocity components and the higher-order moments of the vertical component can be estimated with SF. These characteristics can be estimated with neither CF, nor SP-based techniques. * Contrary to CF, SF are not very sensitive to noise components with a large temporal correlation lag such as ground clutter and point targets. * Using SF-based approach, one can increase signal-to-noise-ratio of received signals by applying highly overlapping receiving antennas. The major shortcomings of the SF-based approach with respect to the CF and SP-based approaches are the following. * SF can be applied only to scalar processes such as the signal's power or amplitude. This results in losing information on the radial (vertical) mean velocity component. * SF are much stronger affected by noise with a zero temporal correlation lag (a white noise) than CF and SP. Therefore, more sophisticated noise treatment is required for SF-based methods than that for CF and SP-based methods. * SF-based approach imposes more restrictive limitations on a SA radar than CF and SP-based approaches. In particular, it requires the receiver centers to be closer to each other, and the sampling interval to be smaller. It is concluded that, depending on measurement conditions, characteristics of a scattering medium can be estimated more effectively with either CF and SP, or SF. The SF-based approach can become a useful alternative to the CF and SP-based approaches, and a combination of several techniques may be optimum.

5.6 IMI.06: Co-located Instruments Simulation by Vemula, Sreenivas

Status of first author: student in poster competition Masters

Authors: Sreenivas Vemula Univ. of Alaska, Fairbanks. ftsv@uaf.edu Denise Thorsen Univ. of Alaska, Fairbanks, ffdt@uaf.edu

Abstract: Co-located instruments used for measuring mesospheric winds often generate vastly different wind estimates. This poster explores a toy model, which simulates the wind estimates for different instruments, given a prescribed wind field. The idea is that by layering known wave structures, i.e., planetary waves, tidal waves, gravity waves, we hope to determine whether the atmosphere itself causes the discrepancies between the instruments and if so identify the parameters that influence the variations in the measurements.

5.7 IMI.07: Rayleigh Lidar Measurements of Temperature and Density by Wang, Weiyuan

Status of first author: student in poster competition Masters

Authors: Weiyuan WANG Graduate Student University of Alaska Fairbanks (UAF) ftww@uaf.edu
 Rich Collins Assistant Professor UAF rlc@gi.alaska.edu

Abstract: The Communications Research Laboratory Rayleigh Lidar measurements of temperature and density have been ongoing at Poker Flat Research Range, Chatanika, Alaska (65N, 147W) since 1997. This poster presents a systematic analysis of the data processing procedures used to determine relative density and temperature profiles from raw lidar photon count profiles. The fundamental source of error or uncertainty in lidar measurements is the intrinsic statistical nature of the photon counting process. In this poster we consider the effects of the retrieval methodology (i.e. estimation of background skylight, spatial filtering or smoothing of the data, and corrections for optical extinction) on the retrievals. We compare the differences that these choices in the retrievals to the uncertainty in the retrievals due to photon counting statistics.

5.8 IMI.08: A Real-Time Preview of the 21st Century Ionosonde by Wright, John

Status of first author: non-student

Authors: J. W. Wright (bill.wright@noaa.gov), R. N. Grubb (Richard.N.Grubb@noaa.gov), and N. A. Zabolin (Nikolay.Zabolin@noaa.gov), Cooperative Institute for Research in Environmental Sciences (CIRES), University of Colorado/NOAA, Boulder, CO, 80309-0216
 M. T. Rietveld (mike.rietveld@eiscat.uit.no), EISCAT Scientific Association, Troms Norway
 F. T. Berkey (ftb@cc.usu.edu), Space Dynamics Laboratory, Utah State University, Logan, UT
 R. C. Livingston (livingston@scion-associates.com), Scion Associates, Port Townsend, WA

Abstract: Modern ionosondes can and should face the challenges posed within the Space-Weather framework, and they must serve expanding research opportunities in geophysics, plasma and radio physics. No longer merely devices for making ionograms, they enjoy the remarkable sensitivity of MF/HF radio to complex plasma structure, in turn exploiting the sensitivity of ionization to nearly every internal and external geophysical influence. Diagnostics in three spatial dimensions, with single-site resolution extending from tens of meters to hundreds of kilometers, with millisecond resolution and unlimited (and adaptive) temporal continuity, can now be demonstrated. Dynamic descriptions of irregular plasma structure are usefully statistical at less than about the Fresnel scale (a few km), and become usefully deterministic toward larger scales.

Fortunately, modern digital technology enables a cost-effective approach to the design of a modern ionosonde, while assuring rapid data processing, dissemination and archival tasks. A new system now in the engineering stage of development will be modular, with at least four parallel, identical, digital receivers, giving at least 20-bit I/Q echo processing with dynamic range exceeding 80 dB. Digital (programmable) definition of output waveform and receiver performance assure echo phase coherence and low RFI generation. An open-source operating system will permit continuing evolution of measurement capabilities for monitoring and research applications.

We demonstrate these extensive ionospheric monitoring and research capabilities with real-time access to the NOAA Dynasondes now operated by EISCAT (Troms Norway) and Utah State University's Bear Lake Observatory:

<http://www.ngdc.noaa.gov/stp/IONO/Dynasonde>

6 Tuesday Evening 17 June 2003 Poster Session Abstracts, Meteor science (other than winds)

6.1 MET.01: Observations of meteor-head echoes using the Jicamarca 50 MHz radar in interferometer mode by Chau, Jorge L.

Status of first author: non-student

Authors: J. L. Chau, R. F. Woodman and M. A. Milla Radio Observatorio de Jicamarca, Instituto Geofisico del Peru, Lima

Abstract: We present results of recent observations of meteor-head echoes obtained with the high power-aperture Jicamarca 50 MHz radar. This type of observations has not been made in the past at Jicamarca, mainly because of the existence of strong equatorial electrojet (EEJ) echoes at similar heights. However, we have recently implemented a new mode that allows us to discriminate meteor-head echoes not only from weak EEJ echoes but also from the strong meteor-trail echoes. We give a detailed description of the technique that allows us to get estimates of the radial velocities (using a matched filter and from the range vs. time relationship of the echo), direction of arrival (using interferometry), absolute geocentric velocities, absolute geocentric decelerations, etc. Statistics are presented for these and other variables for the observations made during the Leonids 2001 and 2002 meteor showers and control days. As it has been observed in other large power-aperture radars, our observations do not show evidence of Leonids meteor shower. Moreover, the distribution of the meteors with respect to the Earth's frame of reference is clustered around the Apex, within ± 10 degrees transverse to the Ecliptic and no more than a few degrees in heliocentric longitude in the Ecliptic plane.

6.2 MET.02: Observations of Sporadic Meteor Events Using the 430 MHz Arecibo Radar by Briczinski, Stanley

Status of first author: student in poster competition PhD

Authors: S.J. Briczinski – Penn State J.D. Mathews – Penn State J.F. Doherty – Penn State C.H. Wen – Penn State

Abstract: The micrometeor observations performed using the 430 MHz Arecibo Observatory Radar have proven to be crucial for the understanding of meteoric effects in the upper atmosphere. Sporadic meteor observations during February of 2001 were analyzed with a FFT periodic search algorithm that automatically detected meteor events. In this poster we present the new technique used to detect meteors as well as the measured parameters (i.e. altitudes, velocities and decelerations) obtained from this method. The results of the new automated technique are compared with previous results.

6.3 MET.03: Meteoric dust effects on Mesospheric Electrodynamics by Gelinás, Lynette

Status of first author: non-student

Authors: L.J. Gelinás, Cornell University, lynett@ece.cornell.edu K.A. Lynch, Dartmouth College, lynch@birkeland.Dartmouth.EDU Richard Collins, University of Alaska, Fairbanks M.C. Kelley, Cornell University, mikek@ece.cornell.edu Peter Mace, Utah State University

Abstract: In March 2002, a series of three rockets were launched from Poker Flat over the course of one night. The rockets made in-situ measurements of charged meteoric dust, electric fields and plasma density during each of the three flights. Ground-based iron and sodium lidars were also used to monitor the neutral atomic metal densities throughout the night. In this paper we present plasma density and electric field data from the three flights, and discuss the role that charged meteoric dust may play in the electrodynamics of the polar mesosphere.

6.4 MET.04: Simulations of Large-Aperature Radar Meteor Observations by Ray, Licia

Status of first author: student in poster competition Undergraduate

Authors: Licia C. Ray Boston University lcray@bu.edu Meers M. Oppenheim Boston University meerso@bu.edu Lars P. Dyrud Boston University ldyrud@bu.edu Kelly D. McMillon Boston University kelspace@bu.edu Sigrid Close Boston University sigrid@ll.mit.edu MIT-Lincoln Labs

Abstract: Large aperture radars frequently detect meteor trails in the E-Region ionosphere between 80-130km. We have constructed a model of meteor processes starting with an ablating meteoroid and ending with the turbulent diffusion of the trail. The input parameters are initial meteoroid mass, composition, velocity, and inclination angle. Ablation, ionization, and expansion models determine the line density of the plasma column created by the meteor. We then use the Farley-Buneman gradient drift instability to establish at which altitudes field-aligned irregularities (FAI) will form. We use this model to simulate large aperture radar RTI images and will present how we expect observations to vary with model and meteoroid parameters. Specifically we will vary the above input parameters, the head echo and trail scattering strength, and display the difference between using Euler and fourth-order Runge Kutta integration techniques.

6.5 MET.05: Signal Processing Techniques for Bursty Interference Removal by Wen, Chun-Hsien

Status of first author: student not in poster competition PhD

Authors: Chun-Hsien Wen, The Pennsylvania State Univ., cxw381@psu.edu John F. Doherty, The Pennsylvania State Univ. jfdoherty@psu.edu John D. Mathews, The Pennsylvania State Univ., jdmathews@psu.edu

Abstract: In this poster, we present signal processing techniques to remove the short-pulse interference of the meteor observation radar data from Arecibo Observatory. We exploit the characteristics of bursty interferences in time domain. Two methods are investigated. First, we calculate the statistical moments of the power profile of received data. When the interference is present in the data, the kurtosis is very high. By checking this parameter, we detect the interference. Second, we apply a nonlinear filter to the power profile of received data. We then compare the power reduction percentage and the standard deviation of the data before and after the filter to detect the presence of the interference. After detecting the interference we blank those corresponding signal samples. Experimental results show that we can efficiently and reliably remove the interference.

7 Tuesday Evening 17 June 2003 Poster Session Abstracts, Lightning / Sprites

7.1 LSP.01: Multi-path D region ionospheric remote sensing by Cheng, Zheng-gang

Status of first author: student in poster competition PhD

Authors: Zhenggang Cheng Duke University zc@ee.duke.edu Steven A. Cummer Duke University cummer@ee.duke.edu

Abstract: In this poster, we report simultaneous multi-location D region ionospheric measurements using very low frequency (VLF) magnetic field waveforms from lightning recorded at Duke University. VLF energy from lightning is almost exclusively reflected below 100 km and thus contains information about the ionospheric D region. Using VLF signals radiated from lightning at multiple locations, received simultaneously at Duke University, we measure the spatial structure of the D region ionosphere over a large geographic region, which has not been made before by other measurements. In this poster, we will also report the investigation of lightning disturbance upon D region ionosphere by comparing D region ionosphere height of a couple of close ionosphere paths that only one of them has some lighting in the path.

7.2 LSP.02: EXPANSION AND ACCELERATION OF STREAMERS IN SPRITES by Liu, Ningyu

Status of first author: student in poster competition PhD

Authors: Ningyu Liu (nul105@psu.edu) and Victor P. Pasko (vpasko@psu.edu)
The Pennsylvania State University

Abstract: Sprites are large luminous discharges, which appear in the altitude range of 40 to 90 km above large thunderstorms [e.g., Sentman et al., GRL, 22, 1205, 1995]. Recent telescopic imaging of sprites revealed an amazing variety of generally vertical fine structure with transverse spatial scales ranging from tens to a few hundreds of meters [Gerken et al., GRL, 27, 2637, 2000; Gerken and Inan, JGR, 107, 10.1029/2002JA009248, 2002; JASTP, 65, 10.1016/S1364-6826(02)00333-4, 2003]. The appearance of the fine structure in sprites has been interpreted in terms of positive and negative streamer coronas, which are considered as scaled analogs of small scale streamers, which exist at high atmospheric pressures at ground level [e.g., Pasko et al., GRL, 25, 2123, 1998; Raizer et al., J. Phys. D Appl. Phys., 31, 3225, 1998; Petrov and Petrova, Tech. Phys., 44, 472, 1999; Pasko et al., GRL, 28, 3821, 2001].

In this talk we report results from a new two-dimensional model, which has recently been developed at Penn State for studies of dynamics of streamers for a wide range of air pressures corresponding to streamer dominated regions of sprites. The model utilizes a modified Scharfetter-Gummel algorithm for solution of electron convection-diffusion equation [Kulikovskiy, J. Comput. Phys., 119, 149, 1995] and accounts for effects of photoionization on the streamer dynamics [e.g., Kulikovskiy, J. Phys. D: Appl. Phys., 33, 1514, 2000, and references therein].

The model results indicate that double headed streamers originating from single electron avalanches in lightning driven quasi-static electric fields at mesospheric altitudes accelerate and expand reaching transverse scales from tens to a few hundreds of meters and propagation speeds up to one tenth of the speed of light, in good agreement with recent telescopic [Gerken et al., 2000; Gerken and Inan, 2002; 2003], high-speed video [Stanley et al., GRL, 26, 3201, 1999; Moudry et al., GRL, 29, 10.1029/2002GL015682, 2002; JASTP, 65, 10.1016/S1364-6826(02)00333-4, 2003] and multi-channel photometric [McHarg et al., JGR, 107, 10.1029/2001JA000283, 2002] measurements of sprites. The pre-ionization of the medium ahead of a streamer by the ionizing UV photons originating from a region of high electric field in the streamer head significantly modifies the streamer scaling properties as a function of air pressure in comparison with those predicted by similarity laws, leading to lower peak electric fields in the streamer head, lower streamer electron densities and wider streamer structures at sprite altitudes 40-90 km, when compared to the ground level. The primary reason for the observed differences is that the effective quenching altitude of the excited states

of the molecular nitrogen that give photoionizing radiation is about 24 km. The quenching of these states is therefore negligible at the sprite altitudes, leading to a substantial enhancement of the electron-ion pair production ahead of the streamer tip due to the photoionization, when compared to the ground level.

7.3 LSP.03: Direction-Finding of Scattered Fields Produced During Non-Ducted LEP Events as Measured at Palmer Station, Antarctica by Moore, Robert

Status of first author: student in poster competition PhD

Authors: Robert Moore, Stanford University, berto@stanford.edu and Umran Inan, Stanford University, inan@nova.stanford.edu

Abstract: Non-ducted Lightning-Induced Electron Precipitation (LEP) Events have been shown to move poleward with time. The particle precipitation associated with these events affect the measured amplitude and phase of Very Low Frequency (VLF) signals propagating beneath the disturbed region. At Palmer Station, Antarctica, the propagation path of the NPM broadcast signal (21.4 kHz, located in Hawaii) is largely latitudinal in the region where lightning-induced electron precipitation is expected to occur. As the precipitation moves poleward, we expect to see a change in the direction of the scattered field received at Palmer Station. The direction of arrival of the scattered field is determined using two crossed-loop magnetic antennas. A study of LEP events measured at Palmer Station is presented.

8 Tuesday Evening 17 June 2003 Poster Session Abstracts, Stratosphere and below

8.1 STR.01: A system study of a troposphere lidar system. by Yue, Jia

Status of first author: student in poster competition Masters

Authors: Jia Yue, Geophysical Institute of University of Alaska, ftjy@uaf.edu; Rich Collins, GI of UAF, rlc@gi.alaska.edu; Nianwen Cao, GI of UAF, ncao@gi.alaska.edu;

Abstract: A tropospheric lidar allows measurement of the aerosol and molecules in the tropospheric region. This poster shows the work done in July 1999 to study a smoldering smoke plume by the frost fire experiment and new work conducted in spring 2003 measuring the troposphere under clear sky conditions. This lidar system is composed of a polarized Nd:YAG laser at 532nm located at Poker Flat Research Range, Alaska(65N, 147W). Except for a change of telescope, the systems are the same. Through comparison of significant differences between the two types of data, the characteristics of the system were identified.

9 Wednesday Evening 18 June 2003 Poster Session Abstracts, Solar-planetary interactions in the upper atmosphere of Earth and other planets

9.1 SPI.01: Examining the effect of different forcing terms to the thermospheric neutral winds by Deng, Yue

Status of first author: student in poster competition PhD

Authors: Yue Deng and Aaron Ridley Center for Space Environment Modeling University of Michigan ydeng@umich.edu

Abstract: To obtain a better understanding of the global thermosphere and ionosphere system, we conduct some numerical experiments using a global ionosphere-thermosphere model (GITM). We run GITM to a roughly steady-state using various strengths of the high-latitude electric potential, F10.7. By varying these parameters, we get what the maximum neutral wind speeds can reach and how long it takes the neutral winds to ramp up. We can gain a quantitative understanding of how the ion drag driven neutral wind varies with altitude, solar cycle, cross polar cap potential. So we are able to quantify the effects of these different forcing terms on the thermosphere-ionosphere system.

9.2 SPI.02: The Solar X-ray Imager (SXI) Occultation Experiment by Hill, Steven

Status of first author: non-student

Authors: Steven M. Hill NOAA/SEC 325 Broadway Boulder, CO 80305 Steven.Hill@noaa.gov
Rodney Viereck NOAA/SEC 325 Broadway Boulder, CO 80305 Rodney.Viereck@noaa.gov

Abstract: Twice a year, for an approximately 40-day period around the equinoxes, the Earth passes in front of the Sun once daily from the vantage point of geostationary orbit. The Solar X-ray Imager (SXI), a routine, operational, patrol instrument for space weather forecasting, is hosted in this orbit by NOAA's GOES 12 satellite. Thus, the SXI offers a unique opportunity to measure the transmission of the lower thermosphere (approximately 100-400 km) in a soft X-ray regime (0.6-6.0 nm) that has remained relatively unexplored. While SXI is a broadband instrument and thus offers little in the way of compositional diagnostics, it has a substantial field-of-view and fine resolution at the line-of-sight tangent point in the atmosphere. During occultations, SXI instantaneously observes an area of about 500 km square with 1 km sampling. Due to relative motion of the Sun, the grid is smeared linearly over 9 km in one dimension. The dimension (vertical vs. horizontal) depends on the occultation geometry. The work presented here represents the first data reduction and analysis from SXI's first eclipse season around the 2003 vernal equinox. Transmission data are computed and registered for a subset of the SXI data. The observed transmissions are compared to results from a model including the solar spectrum, atmospheric structure, species absorption cross sections, and instrument response.

9.3 SPI.03: Photochemical modeling of global variations and ring shadowing in Saturn's ionosphere by Moore, Luke

Status of first author: student in poster competition PhD

Authors: Luke Moore (1), Michael Mendillo (1), Ingo Mueller-Wodarg (1,2)
(1) Center for Space Physics, Boston University (2) Atmospheric Physics Laboratory, University College London

Abstract: A time-dependent photochemical model of Saturn's ionosphere has been developed as an intermediate step towards a fully coupled Saturn-Thermosphere-Ionosphere-Model (STIM). A global circulation model (GCM) of the thermosphere provides the latitude and local time dependent neutral atmosphere. Four

ion species are used (H^+ , H_2^+ , H_3^+ and He^+) with current cross-sections and reaction rates, and the SOLAR2000 model for the Sun's irradiance. Voyager UVS occultation data are adapted to model the UV optical depth radial profile of the rings. Diurnal electron density peak values and heights are generated for all latitudes and seasons under solar minimum and solar maximum conditions, both with and without shadowing from the rings. Photochemical modeling as a first order approach is validated by comparisons between transport and chemical loss time constants in Saturn's ionosphere. In agreement with previous models the ionosphere is dominated by H^+ and H_3^+ . As expected, shadowing from the rings leads to attenuation of solar flux, the magnitude and latitudinal structure of which depends on season. During solstice, the season for the Cassini spacecraft's encounter with Saturn, attenuation has a maximum of two orders of magnitude, causing a reduction in modeled electron densities by as much as a factor of five.

10 Wednesday Evening 18 June 2003 Poster Session Abstracts, Magnetosphere/ionosphere coupling and plasmasphere

10.1 MIC.01: Multivariate Statistical Analysis of Ion Upwelling using Incoherent Scatter Radar Data by Remick, Karen

Status of first author: student in poster competition PhD

Authors:

Abstract: There are a large number of possible acceleration mechanisms which could be responsible for accelerating O⁺ from the ionosphere to the magnetosphere. This study uses multivariate statistical analysis of incoherent scatter radar data in an attempt to identify which of the mechanisms are important.

10.2 MIC.02: Modeling Ionosphere-Thermosphere-Magnetosphere Coupling with the IntegratedSpace Weather Prediction Model (ISM) by Schoendorf, J

Status of first author: non-student

Authors: J. Schoendorf, Mission Research Corporation, Nashua, NH, jschoendorf@mrcnh.com
K. Siebert, Mission Research Corporation, Nashua, NH, ksiebert@mrcnh.com
W. White, Mission Research Corporation, Nashua, NH, bwhite@mrcnh.com

Abstract: Historically, global models of the magnetosphere and ionosphere/thermosphere have operated in isolation, with each type of model treating the other region as a boundary condition. In recent years, existing models have been linked together to create models that cover the entire ionosphere-thermosphere-magnetosphere (I-T-M) system. Unlike these models, the Integrated Space Weather Prediction Model (ISM) is a global first-principles two-material MHD model of the entire I-T-M system with no boundaries between the different regions. The two-material MHD equations, complete with the full Ohm's law including the Hall terms, provide self-consistent electromagnetic and material coupling throughout the ISM computational domain which extends from 40 earth radii (Re) sunward of the earth to 300 Re tailward, and down to a lower ionospheric boundary at approximately 100 km altitude. We describe the model and use currents, electric fields, and ion and neutral velocities to illustrate the I-T-M coupling that is inherent in ISM.

10.3 MIC.03: Comparisons of He⁺ in the plasmasphere with the CTIP model and EUV data from the IMAGE satellite. by Thom, Stuart

Status of first author: student in poster competition PhD

Authors: S.D.Thom: Space and Atmospheric Group, University of Sheffield, s.thom@shef.ac.uk
C.R.Wilford: Space and Atmospheric Group, University of Sheffield, c.wilford@sheffield.ac.uk
G.J.Bailey: Space and Atmospheric Group, University of Sheffield, g.bailey@sheffield.ac.uk
B.R.Sandel: Lunar and Planetary Laboratory, University of Arizona, USA, sandel@vega.LPL.Arizona.EDU

Abstract: Helium ions in the Earth's plasmasphere resonantly scatter solar radiation at 30.4nm. The Extreme Ultraviolet Imager (EUV) of the IMAGE (Imager for Magnetopause-to-Aurora Global Exploration) mission studies the global distribution of He⁺ by detecting these emissions. We use a coupled thermosphere-ionosphere-plasmasphere model (CTIP) to solve the equations of continuity, momentum and energy balance for O⁺, H⁺ and more importantly for this investigation, He⁺. Model results are compared to IMAGE EUV data on a global scale.

11 Wednesday Evening 18 June 2003 Poster Session Abstracts, Long term variations of the upper atmosphere

11.1 LTV.01: INITIAL SCIENCE PLANS FOR CAWSES (CLIMATE AND WEATHER OF THE SUN-EARTH SYSTEM): REQUEST FOR IDEAS AND INPUTS by Basu, Sunanda

Status of first author: non-student

Authors: Sunanda Basu (1), Janet U. Kozyra (2), CAWSES SSG Team and Theme Leaders (1) Center for Space Physics, Boston University (sbasu@bu.edu or sbasu@ssd5.nrl.navy.mil), (2) Space Physics Research Lab, University of Michigan, Ann Arbor, MI 48109 (phone 734-647-3550, fax 734-647-3083, jukozyra@engin.umich.edu)

Abstract: During 2004-2008, Climate and Weather of the Sun-Earth System (CAWSES), SCOSTEP's new international scientific program, will link the world's scientists in a cooperative effort to study the entire interactive Sun-Earth system. With this new program, SCOSTEP seeks to provide coordination across the international scientific community for cooperative studies that draw together data from past, present, and planned space missions; ground-based observations; and theory, modeling, and data analysis efforts to produce improvements in space weather forecasting, design of space- and Earth-based technological systems, and increased understanding of the role of solar-terrestrial influences on Global Change. In 2003, preceding the initiation of CAWSES, serious consideration is being given to plans for the strategic implementation of both near-term and overarching program goals. Four themes were chosen which focus scientific activities. These are: Solar Influence on Climate, Space Weather: Science and Applications, Atmospheric Coupling Processes and Space Climatology. Theme leaders in each area are engaged in developing initial science plans with the participation of the international scientific community in discipline areas that span the entire system from the sun to the Earth's middle atmosphere. The aim of this poster is to update the CEDAR community on the CAWSES goals, objectives and initial implementation plans and solicit new ideas, comments and suggestions for the next revision of science plans to be discussed at the June 30 July 11, 2003 IUGG meeting in Sapporo, Japan.

11.2 LTV.02: Online Database for Thermal Ionospheric Plasma Data from DMSP by Hairston, Marc

Status of first author: non-student

Authors: Marc Hairston (hairston@utdallas.edu) Robin Coley (coley@utdallas.edu) Kelly Drake (classiccat63@yahoo.com) all at Center for Space Sciences University of Texas at Dallas

Abstract: Since 1987 the polar orbiting DMSP weather satellites have carried a set of thermal plasma instruments built by the University of Texas at Dallas. These instruments (a retarding potential analyzer, ion drift meter, Langmuir probe, and scintillation meter) provide data about the bulk ion velocity vector, ion density, ion composition, ion temperature and electron temperature in the topside ionosphere at an altitude of about 840 km. We have created an online website at <http://cindispace.utdallas.edu/DMSP/> where researchers can obtain these data in both graphical and numerical form. This poster describes the data, the website, the features researchers can use to access the dataset, and the quality flags we have used to classify the data.

11.3 LTV.03: The analysis of TEC data from TOPEX/Poseidon mission by Jee, Geonhwa

Status of first author: student in poster competition PhD

Authors: Geonhwa Jee, Robert W. Schunk and Ludger Scherliess

Abstract: TOPEX/Poseidon mission has provided an extensive database of vertical TEC over the oceans that covers the period from August 1992 to the end of 2001. This database was analyzed in order to study the TEC climatology that is inherent in the data. Since the database covers nearly a full solar cycle, it was possible to elucidate the TEC variation with changes in the solar flux (F10.7 cm). First, longitudinally-averaged TEC data were examined and these data were binned by season (equinox, June and December solstice), geomagnetic activity (low, medium, and high Kp), and solar flux (low and high F10.7 cm flux), with 1 by 1 deg. bins in geomagnetic latitude and magnetic local time (4-minute bin). The annual and semiannual anomalies are clearly seen, but the analysis does not show the seasonal anomaly because of the longitudinally-averaged binning. The equatorial anomaly is the most prominent feature in the TEC maps and they show the TEC variations with geomagnetic and solar activity. The effects of changes in the solar flux are very large. Compared with the low solar flux condition (F10.7 \leq 120), the TEC values at high solar flux (F10.7 \geq 120) are much larger (about 100%) and the equatorial anomaly lasts longer into the night, up to midnight. With regard to the effects of geomagnetic activity, the TEC maps show some features of ionospheric storms. Generally, the positive phase of the ionospheric storm appears at midlatitudes, but the low-latitude ionosphere displays negative phases. At solstice, the summer hemisphere displays positive and negative phases, but the phase tends to be positive in the winter hemisphere. However, the effects are not as large as the solar activity effects, probably because the Kp bins in this study don't represent real storm periods. Finally, three longitudinal bins were added in order to see how the TEC morphology varies with longitude; Indian (30 \leq 150 deg.), Pacific (150 \leq 280 deg.), and Atlantic (280 \leq 30 deg.) geographic longitude bins were added. The TEC measurements display a strong longitudinal variation that closely follows the longitudinal variation of the magnetic declination. In southern Pacific sector, where the declination is positive and large, the TEC variation in magnetic local time is significantly different than the variation in the other longitude sectors, where the magnetic declination is negative in the southern hemisphere. Also, at noon, the longitudinal variation of TEC is typically opposite to that at midnight.

11.4 LTV.04: Climatology of Extreme Upper Atmospheric Heating Events by Knipp, Delores

Status of first author: non-student

Authors: D. J. Knipp, T. Welliver, M.G. McHarg, F. K. Chun, Department of Physics, US Air Force Academy, CO, 80840, USA, W. K. Tobiska Space Environment Technologies, 1676 Palisades Dr., Pacific Palisades, CA, 90272, USA, D. Evans NOAA Space Environment Center R/E/E, 325 Broadway, Boulder, CO, 80303, USA

Abstract: We use a trio of empirical models to estimate the relative contributions of solar extreme ultraviolet (EUV) heating, Joule heating and particle heating to the global energy budget of the earth's upper atmosphere. Daily power values are derived from the models for the three heat sources. The SOLAR2000 solar irradiance specification model provides estimates of the daily extreme EUV solar power input. Geomagnetic power comes from a combination of satellite-derived particle precipitation power and an empirical model of Joule power derived from hemispherically-integrated estimates of high-latitude heating, which we discuss in this paper. From 1975 to mid-2002 the average daily contributions were particles: 51 GW, Joule: 95 GW and solar: 784 GW. Joule and particle heating combine to provide more than 15% of the total global upper atmospheric heating and approximately one third of the variability in the heating. For the top ten percent and top one percent of heating events, contributions rise to 20% and 25% respectively. In the top 15 heating events geomagnetic power contributed more than 50% of the total power budget. During three events the Joule power alone exceeded solar power.

11.5 LTV.05: Towards a Determination of Thermospheric and Exospheric Hydrogen Densities from Coincident Ground-Based and Satellite Airglow Data by Mierkiewicz, Edwin

Status of first author: non-student

Authors: Edwin J. Mierkiewicz (emierk@wisp.physics.wisc.edu), Department of Physics, University of Wisconsin, Madison, WI
 James Bishop (jbishop@uap2.nrl.navy.mil), E.O. Hulburt Center for Space Research, Naval Research Laboratory, Washington, D.C.
 Fred L. Roesler (roesler@wisp.physics.wisc.edu), Department of Physics, University of Wisconsin, Madison, WI
 Jose Francisco Gomez (jfg@laeff.esa.es), Laboratorio de Astrofisica Espacial y Fisica Fundamental/INTA, Madrid, Spain
 Susan Nossal (nossal@wisp.physics.wisc.edu), Department of Physics, University of Wisconsin, Madison, WI

Abstract: Atomic hydrogen plays several unique roles in the terrestrial atmosphere. For example, as a daughter of the important mesospheric minor species H₂O and CH₄, knowledge of the MLT atomic hydrogen density distribution and associated vertical flux may prove to be valuable in understanding the chemistry in the MLT region.

Recent advances in Fabry-Perot instrumentation (e.g., annular summing spectroscopy) have greatly increased the quality and quantity of ground-based geocoronal Balmer series emission data. Extensive Balmer alpha and beta data sets have been obtained with two large aperture (15 cm), double-etalon, Fabry-Perot spectrometers located at Pine Bluff, WI (PBO) and at Kitt Peak, AZ (WHAM). Absolute intensity calibration has been made through same-night observations of well-established astronomical objects (nebulae). Complementing these measurements, recent satellite missions have provided large sets of FUV and EUV emission data, including Lyman line intensities. The EURD instrument on the Spanish satellite MiniSat-1, which measured the diffuse interstellar radiation field in 1997-2001, has provided numerous data sets coincident with our ground-based measurements.

Coincident Balmer alpha (PBO) and Lyman beta (EURD) observations for early March 2000 are presented. The Balmer alpha and Lyman beta intensity measurements, through their intensity variations with solar depression angle and viewing geometry, provide tight constraints on thermospheric and exospheric atomic hydrogen abundances. An analysis procedure for handling large data sets from different instruments is being developed for determining atomic hydrogen density distributions; example results of this procedure are described, involving searches through an extensive set of lyao_rt predictions systematically covering large ranges of relevant parameter values.

In addition, the PBO Fabry-Perot operates at a resolving power (85,000) which is sufficient to allow a detailed investigation of the Balmer alpha line shape. A significant decrease in Balmer alpha Doppler width with increasing shadow altitude is detected. Preliminary applications of lyao_rt indicate good agreement with Doppler width trends in the nonisothermal geocorona.

This work is funded by the National Science Foundation through grants ATM-9908775, ATM-0003166, AST96-19424 and AST02-04973.

11.6 LTV.06: Exploration of Trends in the Wisconsin Long Term Record of Thermospheric+Exospheric H-alpha Column Emission Intensities by Nossal, Susan

Status of first author: non-student

Authors: S.M. Nossal, Dept. of Physics, University of Wisconsin-Madison, nossal@wisp.physics.wisc.edu
 F.L. Roesler, Dept. of Physics, Univ. of Wisconsin-Madison, roesler@wisp.physics.wisc.edu
 E.J. Mierkiewicz, Dept. of Physics, Univ. of Wisconsin-Madison, emierk@wisp.physics.wisc.edu
 J. Bishop, E.O. Hulburt Center for Space Research, Naval Research Laboratory, jbishop@uap2.nrl.navy.mil
 R.J. Reynolds, Dept. of Astronomy, Univ. of Wisconsin-Madison, reynolds@astro.wisc.edu

Abstract: Upward fluxes of hydrogen containing molecules such as methane, water vapor, and molecular hydrogen are the primary source of hydrogen-containing chemical species in the middle and upper atmosphere. Understanding the sensitivity of the thermosphere+exosphere to hydrogenous species distributions below, to sources of natural variability, and to possible long term climatic changes are central questions for geocoronal research.

Observations of thermospheric+exospheric H-alpha column emissions by the Wisconsin H-alpha Mapper (WHAM) Fabry-Perot over the 1997-2001 rise in the solar cycle are the first Wisconsin-based observations to show a statistically significant solar cyclical variation in the geocoronal H-alpha emission, with higher emissions during solar maximum periods. This variation is small compared with variations in the hydrogen exobase density and the solar excitation flux over the solar cycle. The WHAM observations corroborate suggestions of a solar cyclic trend seen in past mid latitude Wisconsin-based H-alpha observations. Collectively, this long term, consistently calibrated data record now spans two solar cycles.

We will present evidence for a solar cyclical trend in the Wisconsin long term data record, and will discuss these data in the context of the 30-50% increase in exospheric hydrogen predicted to result from a doubling of tropospheric methane and carbon dioxide concentrations [Ehhalt, 1986; Roble and Dickinson, 1989]. We will also discuss hydrogen column abundance retrieval from the H-alpha emission observations.

11.7 LTV.07: Long Duration Incoherent Scatter Data Sets by Van Eyken, Tony

Status of first author: non-student

Authors: A van Eyken (Tony.van.Eyken@eiscat.com), EISCAT Scientific Association, Kiruna, Sweden, J M holt (jmh@haystack.mit.edu) and S Zhang (shunrong@haystack.mit.edu), MIT Haystack Observatory, Westford MA 01886, USA

Abstract: Recent developments in Incoherent Scatter radar hardware, coding techniques, data processing and data distribution make the recording of extended datasets both practical and valuable. A number of Incoherent Scatter radars, including the Millstoe Hill Radar near Boston and the EISCAT Svalbard Radar near Longyearbyen, have developed the infrastructure to support long experiments and can already handle programmes with durations of two to four weeks (or more). Long duration experiments provide possibilities to study phenomena not normally accessible to these facilities and also provide datasets applicable to comparison with many ionospheric and atmospheric models. The ready availability of fully analysed data through WWW-based database tools allows these data to be easily exploited by a wide user community.

11.8 LTV.08: Millstone Hill ISR Long-Duration Experiments - Preliminary Analysis by Zhang, Shun-Rong

Status of first author: non-student

Authors: Shun-Rong Zhang (shunrong@haystack.mit.edu) John M. Holt (jmh@haystack.mit.edu) Phil J. Erickson (pje@haystack.mit.edu) Frank Lind (flind@haystack.mit.edu) Larisa Goncharenko (lpg@haystack.mit.edu) William Rideout (brideout@haystack.mit.edu) Glenn Campbell (grc@haystack.mit.edu), MIT Haystack Observatory, USA, and Tony van Eyken (Tony.van.Eyken@eiscat.com), EISCAT Scientific Association, Kiruna, Sweden,

Abstract: From October 4 to November 4, 2002, the EISCAT Svalbard Radar and Millstone Hill Radar operated for 32 consecutive days. This was the longest-duration run ever attempted by an incoherent scatter radar. The Millstone Hill measurements were carried out with the 68 m zenith antenna, providing a continuous dataset of basic ISR parameters Ne, Te, Ti, and V0 (line-of-sight velocity) with a high time resolution (4 min). Interleaved 480 usec single-pulse and alternating codes were utilized for most of the experiment. The alternating-code observations yielded data from 100 to 700 km with a high range resolution.

The long-duration experiment provided a unique opportunity to study a number of ionosphere-thermosphere phenomena which normally cannot be addressed, e.g., to investigate possible planetary wave signatures and their development with altitude in the ionosphere and thermosphere, to study ionospheric variability, especially its altitude dependences for parameters such as plasma temperature and ion drift which can only be obtained with ISRs, and to perform data modeling and assimilation tests.

12 Wednesday Evening 18 June 2003 Poster Session Abstracts, Polar dynamics and aeronomy

12.1 POL.01: Evaluation of Statistical Convection Patterns For Real-Time Ionospheric Specifications and Forecasts by Bekerat, Hamed

Status of first author: student in poster competition PhD

Authors: Hamed A. Bekerat, Robert W. Schunk, and Ludger Scherliess
Center for Atmospheric and Space Sciences Utah State University Logan, UT 84322-4405

Abstract: Abstract Statistical models of high-latitude plasma convection have been used in a wide range of studies pertaining to the ionosphere and thermosphere and they are beginning to be used in various space weather applications. However, the statistical convection models only provide average, not instantaneous, convection patterns, and it is not clear if they are real convection patterns or blurred images of convection. It is also unclear how reliable these convection models are for applications involving ionosphere-thermosphere specifications and forecasts. To address these issues, a quantitative analysis was conducted of the Weimer [2001] empirical convection model, which is the most comprehensive model of high-latitude convection that has been constructed to date. First, criteria were established to determine whether or not a modeled convection pattern was correct for a given set of geophysical conditions. The criteria adopted were reasonable, but stringent. Then, the cross-track ion drift velocities obtained from Weimer [2001] were compared with the corresponding velocities measured by the DMSP F13 satellite. The comparisons were done for nearly a year (1998) of satellite crossings of the northern polar region (4430 successive crossings). The results indicate that the Weimer [2001] model is able to produce the gross structure in the convection pattern, i.e., it is good in a statistical sense. However, it does not adequately capture the mesoscale spatial structure and convection magnitudes observed by the DMSP satellite. Typically, it was able to capture real (instantaneous) convection features in only about 3% of the satellite crossings. These results have important implications for using empirical convection models in space weather applications.

12.2 POL.02: Convective behaviour and growth of E-region HF irregularities by Drexler, Josef

Status of first author: student in poster competition PhD

Authors: J. Drexler, U of Western Ontario, jdrexler@uwo.ca J.-P. St.-Maurice, U of Western Ontario, jstmauri@uwo.ca

Abstract: HF regularities in the E-region can have a vertical (parallel) group velocity that is several orders of magnitude larger than the ExB drift. This vertical motion may dominate the evolution of the waves, through convection into and out of the unstable region.

In addition to changes in the growth rate at various heights, conservation of wave energy requires that the perturbed density changes proportionally to the square root of the background plasma density. This leads to an additional apparent growth of the waves—very similar to the growth of internal gravity waves—that can also dominate the wave evolution. As a result, the traditional local gradient drift growth rate has little or no influence on the wave amplitude.

We will show how the large vertical group velocity necessarily arises from the altitude dependence of the neutral density. This is associated with the fact that the frequency is a function of altitude. From this altitude dependence of the frequency, we can then determine the parallel wave number and the aspect angle as a predictable function of time. We will present numerical calculations of the wave amplitude which show the surprising result that the altitude and phase speed of the peak amplitude are different depending on whether we are interested in the amplitude of the perturbed density, or the fraction of the density perturbation.

12.3 POL.03: Joule heat calculations, standard deviations, and cross-correlations derived from the Dynamics Explorer-2 satellite by Emery, Barbara

Status of first author: non-student

Authors: Barbara Emery, HAO/NCAR, emery@ucar.edu and Arthur Richmond, HAO/NCAR, richmond@ucar.edu

Abstract: The Dynamics Explorer-2 satellite measured the in-situ auroral electron precipitation, ion drifts and magnetic perturbations from day 249 in 1981 to day 47 in 1983. These are used to analyze the statistical properties of auroral precipitation, ionospheric conductances, electric field strength, Joule heating, and the Poynting vector. Over the two year period, 2895 polar cap passes are binned in 2.5 and 5.0 degrees of magnetic latitude and approximately equal area magnetic local time for different hemispheric, seasonal and magnetic activity conditions. The standard deviations are often larger than the averages. The distribution of Joule heating (QJ) resembles that of the electric field squared (E2), with extra Joule heat on the dayside due to the solar conductance. The Poynting vector was only found for 30% of the passes, and so was often less than the average Joule heat from many more passes. However, the subset of Joule heat found when the Poynting vector existed, showed that while similar, the Poynting vector had larger values and larger standard deviations compared to the Joule heat.

Since $QJ = Ped \times E2$, we examine the cross-correlations between the electric field squared (E2) and the total Pedersen conductance (Ped). Longitudinal peaks in E2 and in the auroral Ped are often anticorrelated, with some latitudinal offset, especially on the dawn side. These anti-correlations and offsets lead to small scale cross-correlations (≈ 250 km or ≈ 500 km) that are mostly negative poleward of the auroral peaks, with more negative cross-correlations for the 2.5 magnetic latitude bins. Large scale cross-correlations (250 x 250 km or 500 x 500 km) are mostly positive, except just poleward of the auroral zone, that expanded on the dusk side with the smaller grid size, with winter polar averages decreasing by 0.07 for the smaller grid. Values are ± 0.30 , or less than 30% in areas of significant Joule heating. Total cross-correlations are smaller, with net polar averages between -0.02 and +0.07 for a bin size of 2.5 mlat, compared to between -0.06 and +0.09 for 5.0 mlat bins.

The small total cross-correlations tended to reduce the standard deviation on the dawn side from negative correlations, and to increase them on the dusk side from positive correlations, but only slightly. The standard deviations in the bins from the product of the standard deviations of E2 and Ped were still much smaller than the standard deviations of QJ, with or without the cross-correlation terms.

12.4 POL.04: Monte Carlo Simulation for the Spreading Effect of an Auroral Proton Beam by Fang, Xiaohua

Status of first author: student in poster competition PhD

Authors: Xiaohua Fang, University of Michigan, xhfang@umich.edu; Michael W. Liemohn, University of Michigan, liemohn@umich.edu; Janet U. Kozyra, University of Michigan, jukozyra@srvr5.engin.umich.edu; Stanley C. Solomon, High Altitude Observatory, NCAR, stans@ucar.edu.

Abstract: A 3D Monte Carlo model has been developed to study the beam spreading effect of incident energetic auroral protons during their precipitation in the Earth upper atmosphere. Energetic protons with an isotropic angular distribution impact at 700 km altitude. Two types of incident energy spectra, monoenergetic and Maxwellian distribution, are considered. Interaction of the fast particles with a 3-species atmosphere (N₂, O₂ and O) is included through charge exchange, electron stripping, ionization, excitation and elastic scattering collisions. A uniform geomagnetic field is assumed in the model. It is found that the main dispersion region for precipitating protons is located in the altitude range of 300-400 km, where the first few charge exchange collisions play significant roles. For monoenergetic injection with 1-100 keV energy, the particle beam widths vary from 250 km to 50 km within which 80% particles are confined. The beam radii according to primary ionization rates are much wider than those of the downward particles, since the average particle flying angle with respect to the vertical direction increases away from the central region, which makes the ionization probability rise. A Maxwellian energy distribution gives nearly the same results as a monoenergetic spectra of the same characteristic energy, but with a narrower beam radii. In the case that the geomagnetic field lines are tilted, asymmetric spreading is demonstrated.

12.5 POL.05: Theoretical Investigation of High-Latitude Outflow for Ions and Neutrals by Gardner, L

Status of first author: student in poster competition PhD

Authors: L. C. Gardner, Utah State University, larry.gradner@usu.edu R. W. Schunk, Utah State University, schunk@cc.usu.edu

Abstract: The outflow of thermal ions from the high-latitude Polar Regions has been extensively studied over the past several decades. The study of the impact of energetic neutral atoms, however, is a relatively new field of study. A new model based on the Flux Corrected Method has been developed and incorporates the relevant charge exchange chemistry appropriate for the high-latitude ionosphere. The model then uses this chemistry to determine the characteristics of the ions and neutral streams through the use of independent continuity and momentum equations for each species of interest. In this study the ions of interest are H⁺ and O⁺, and the neutral stream species are Hs and Os, with the neutral background being supplied by the MSIS model.

12.6 POL.06: MESO-SCALE VELOCITY STRUCTURE IN THE HIGH LATITUDE F-REGION by Johnson, Eric

Status of first author: student not in poster competition PhD

Authors: 1. Eric Johnson, The University of Texas at Dallas, ejohnson@utdallas.edu
2. Dr. Roderick Heelis, The University of Texas at Dallas, heelis@utdallas.edu

Abstract: At high latitudes in the F-region the bulk ion flow is driven predominantly by electric fields originating in the magnetosphere and magnetosheath. During times of southward IMF and large-scale 2-cell convection pattern usually prevails with convection cells with characteristic spatial scales of 1000 km (10 degrees of latitude). In addition to this large-scale convection feature there exist smaller scale velocity structures with scale sizes ranging from 100s of km to a 10s of meters. At the smallest scales the structure is most relevant to the formation of plasma waves and instabilities and does not have a significant effect on the bulk plasma temperature or the neutral atmosphere motions. However, at intermediate scales between 1 km and 100 km the ion velocity structure can have a significant impact on the ion temperature and perhaps the neutral gas velocity. Here we report on an initial study of the characteristics of ion velocity structure in this scale size range. We examine the magnitude of the structure and its relationships to the bulk flow in the ion and neutral gas as well as the ion temperature. Once established these relationships can be used to construct an empirical model of the structure that can be tested in coupled ionosphere thermosphere models.

12.7 POL.07: Climatological Characteristics of the Polar Ionosphere Based on the Sondrestrom and Chatanika Incoherent Scatter Radar Measurements by Kwak, Young-Sil

Status of first author: student in poster competition PhD

Authors: Y.-S. Kwak, Kyungpook National University, Daegu, Korea, ys-kwak@hanmail.net, B.-H. Ahn, Kyungpook National University, Daegu, Korea, bhahn@knu.ac.kr, B. A. Emery, High Altitude Observatory, NCAR, Boulder, CO, emery@hao.ucar.edu, J. P. Thayer, SRI International, Menlo Park, CA, thayer@sri.com, M. McCready, SRI International, Menlo Park, CA, Mary.McCready@sri.com, J. Watermann, Solar-Terrestrial Physics Division, Danish Meteorological Institute, Copenhagen, Denmark, jfw@dmi.dk

Abstract: The climatological characteristics of the polar ionosphere is examined in terms of the ionospheric conductance and electric field. For this purpose, 109 and 43 days of measurements from the Sondrestrom and Chatanika incoherent scatter radars, respectively, are utilized. By combining the conductance and electric field, it is possible to deduce the overhead ionospheric current distributions. The ionospheric current density, thus obtained, is compared with the corresponding ground magnetic disturbance. Also examined is the global

field-aligned current affecting the ground magnetic disturbance, particularly on the D component. Several interesting characteristics about the polar ionosphere are apparent from this study: (1) The sun determines largely the conductance over Sondrestrom, while the nighttime conductance distribution over Chatanika is significantly affected by auroral precipitation. (2) The regions of the maximum N-S electric field over Chatanika are located approximately at the dawn and dusk sectors, while they tend to shift towards dayside over Sondrestrom. The E-W component over Chatanika is negligible compared to that of Sondrestrom. (3) The E-W ionospheric current over Chatanika flows dominantly in the night hemisphere, while it flows in the sunlit hemisphere over Sondrestrom. The N-S current over Chatanika flows prominently in the dawn and dusk sectors, while a strong southward current flows over Sondrestrom in the prenoon sector. (4) The assumption of infinite sheet current approximation is far from realistic, underestimating the current density by a factor of 2 or more. It is particularly serious for higher latitude region and during quiet period. (5) The correlation between DH and JE is higher than the one between DD and JN, indicating that field-aligned current (FAC) affects significantly DD. (6) Total global FAC over Chatanika and Sondrestrom are quite comparable. With enhancement of magnetic activity, FAC increases drastically over Chatanika by a factor of 4 or 5 but the increment is insignificant over Sondrestrom.

12.8 POL.08: Ion temperature maximum appeared in the polar E-F transition region by OYAMA, SHIN-ICHIRO

Status of first author: non-student

Authors: Shin-ichiro Oyama: Geophysical Institute, University of Alaska Fairbanks, USA, soyama@gi.alaska.edu Brenton J. Watkins: Geophysical Institute, University of Alaska Fairbanks, USA, ffbjw@uaf.edu Sawako Maeda: Kyoto Women's University, Japan, smaeda@kyoto-wu.ac.jp Hiroyuki Shinagawa: Solar-Terrestrial Environment Laboratory, Nagoya University, Japan, shinagawa@stelab.nagoya-u.ac.jp

Abstract: Day-night differences of ion temperature in the polar ionosphere (from 100 to 300 km) have been determined using the European Incoherent Scatter (EISCAT) radar data for solar maximum geomagnetically quiet summer conditions. The hourly mean ion temperature at local noon shows a maximum at 190 km, while at local night does not show it. These results are not in agreement with standard model profiles of ion temperature. In this study we use data obtained during geomagnetically quiet conditions ($A_p \leq 20$) in summer (June and July) from 1990 to 1992 (solar maximum period) in a height region from 100 to 300 km with the EISCAT UHF radar operating in CP-1 mode. The CP-1 mode uses the UHF radar at Tromsø, Norway (931 MHz; 69.35 N, 19.14 E, 66.12 invariant latitude; $LT = UT + 1 \text{ hr } 15 \text{ min}$ and $MLT = UT + 3 \text{ hr } 15 \text{ min}$) to observe the field-aligned ionospheric parameters (electron density, ion and electron temperatures, and line-of-sight ion velocity). The time resolution used here is 5 min. The height resolution is 3 km below 150 km, and 22 km above this height. We have selected 7 successive data segments covering a 24-hour interval beginning at 1200 UT. We derive the mean values of ion temperature using a weighting function assumed the error values estimated by GUISDAP (Grand Unified Incoherent Scatter Design and Analysis Package) that is employed on the incoherent scatter spectra to derive data used for this study. The ion temperature at high latitudes is determined principally by frictional heating and by heat exchange with the neutrals and electrons. In the presentation, we will discuss effects of frictional heating on the ion temperature maximum. Future work will investigate possible similar high-latitude effects at the Sondrestrom observatory.

12.9 POL.09: High-Latitude Joule Heating Rates Using Different Electric Field Models During the May 1998 Storm by Ridley, Aaron

Status of first author: non-student

Authors: Aaron Ridley and Yue Deng Center for Space Environment Modeling University of Michigan ridley@umich.edu

Abstract: We present results from the newly created global ionosphere thermosphere model of the May 1998 magnetic storm. We have run this storm using a number of different electric field models, such as AMIE

and Weimer [1996]. In addition, we have used 1, 2, 5, 10, and 15 minute average electric field patterns to determine the quantitative effect of temporal variation in the electric field on the high-latitude Joule heating. We examine integrated Joule heating over the entire high-latitude region, and integrals over each altitude layer to determine the effect at different layers.

12.10 POL.10: Electrodynamic Characteristics of the Duskside Branch of the Two-Cell Aurora by Shue, Jih-Hong

Status of first author: non-student

Authors: J.-H. Shue, JHU/APL, shuej1@oval.jhuapl.edu, P. T. Newell, JHU/APL, Patrick.Newell@jhuapl.edu, K. Liou, JHU/APL, Kan.Liou@jhuapl.edu, C.-I. Meng, JHU/APL, Ching.Meng@jhuapl.edu, G. A. Germany, CSPAR, UAH, germanyg@cspar.uah.edu, M. R. Hairston, CSS, UTD, hairston@utdallas.edu, F. J. Rich, AFRL, Hanscom AFB, frederick.rich@hanscom.af.mil, G. K. Parks, SSL, UCB, parks@ssl.berkeley.edu.

Abstract: The characteristic of the two-cell aurora is azimuthal elongation over extended local times with gaps at noon and midnight. Its electrodynamic association with the convection, particle precipitation, and field-aligned currents has not been fully understood. In conjunctions with DMSP F12 spacecraft on the duskside branch of the aurora, we are able to investigate the association of the auroral emissions with electric fields, upward field-aligned currents, and energy flux of electrons. With a comparison of the peaks of Polar Ultraviolet Imager Lyman-Birge-Hopfield long (LBH-long) auroral emissions and DMSP electron energy flux, we find that there exists a 2.3 degree systematic latitudinal offset between the peak energy flux and peak LBH-long. A calibration of this offset has been performed by simply shifting the location of the peak LBH-long to that of the peak energy flux. Results show that the duskside branch of the two-cell aurora is associated with one or several discrete electron precipitation occurring in the region 1 field-aligned currents. Associated features of the electric fields are consistent with the typical two-cell convection pattern. The intensity of auroral emissions is changing in the poleward portion of the auroral oval during periods of no substorms. However, the intensity is changing in the equatorward portion of the auroral oval during period of substorms.

13 Wednesday Evening 18 June 2003 Poster Session Abstracts, Mid-latitude thermosphere and ionosphere

13.1 MTI.01: The Sporadic E Layer Instability by Cosgrove, Russell presented by Heinselman, Craig

Status of first author: non-student

Authors: Russell B. Cosgrove Roland T. Tsunoda

Abstract: Sporadic E (Es) layers are layers of long lived metallic ions that form at around 100 km in altitude. The wind shear theory for the layer formation has been around for over forty years. However, certain features of Es layers have defied interpretation, such as their tendency to organize into frontal structures with a peculiar northwest to southeast frontal alignment, and the phenomenon of quasi-periodic (QP) echoes. The latter are coherent radar echoes with broad doppler spreads, suggesting large electric fields. The anomalous observations suggest a role for electrodymanics in Es layers that has hitherto gone undescribed. Below, we describe our finding that the configuration of a Es layer at a wind shear node is in fact unstable at night, due to electrodymanical forces. The growth rate for the instability maximizes for plane wave perturbations with phase fronts aligned northwest to southeast, which would seem to explain the observation of frontal structures. The growth of perturbations involves strong polarization electric fields, which may provide an explanation for QP echoes.

13.2 MTI.02: Thermospheric winds derived from the MU radar incoherent scatter observations by Kawamura, Seiji

Status of first author: non-student

Authors: Seiji Kawamura, Communications Research Laboratory, s-kawamura@crl.go.jp, Shoichiro Fukao, Radio Science Center for Space and Atmosphere, Kyoto University, fukao@kurasc.kyoto-u.ac.jp

Abstract: The MU radar at Shigaraki (34.85N, 136.10E; magnetic latitude 25N) in Japan is a unique radar which can perform incoherent scatter measurements in the Asian sector. The time-of-day, day-of-year, solar activity, and geomagnetic activity behavior of meridional thermospheric winds are studied as climatological averages using the MU radar incoherent scatter observations during 11 years. The basic character of the thermospheric wind is well explained by a diurnal flow around the globe from the dayside pressure maximum to the nightside pressure minimum superposed on smaller flow from the summer to the winter hemisphere. The speed of this flow and many of its characteristics are strongly regulated by ion drag. Millstone Hill, Saint Santin, and MU winds are quite similar for high solar activity, while Millstone winds for low solar activity are affected by high latitude energy input. The geomagnetically disturbed wind is generally more southward (or less northward) than the quiet winds, which shows that, even at the low magnetic latitude of the MU radar (25N), substantial shifts in the background wind are impressed by high-latitude heating. Meridional thermospheric winds affect on the yearly variations of the ionosphere directly and indirectly. We will also discuss how the meridional thermospheric wind affects on the yearly variations of the electron density and electron/ion temperatures.

13.3 MTI.03: Comparison of ionospheric dynamo currents and magnetic per- turbations modeled by the TIEGCM with CM3e model results by Maute, Astrid

Status of first author: non-student

Authors: Astrid I. Maute, Arthur D. Richmond National Center for Atmospheric Research, HAO, Boulder, CO, USA maute@ucar.edu richmond@ucar.edu

Terence J. Sabaka Raytheon ITSS, Lanham, MD, USA sabaka@geomag.gsfc.nasa.gov

Nils Olsen Danish Space Research Institute, Copenhagen, Denmark nio@dsri.dk

Abstract: The National Center for Atmospheric Research Thermosphere-Ionosphere-Electrodynamics General-Circulation Model (TIEGCM) is used to study the spatial and universal-time variations of electric currents generated by the ionospheric wind dynamo, and their associated geomagnetic perturbations at the ground and at low-Earth-orbit (LEO) altitudes.

We will compare the magnetic perturbations from the model for quiet time conditions at low and middle latitudes with observations to evaluate the quality of the model results. We will also use the extended geomagnetic Comprehensive Model Phase 3 (CM3e) for comparison with the magnetic field perturbations derived from TIEGCM. The CM3e models the core and crustal fields as well as the regular, quiet-time near-Earth magnetic perturbation field by using measurements from Magsat, POGO, Oersted and CHAMP and from ground observatories. The CM3e separates the magnetic perturbation field into core, crustal, ionospheric and magnetospheric components and can also be used to validate the ionospheric component predicted by the TIEGCM.

We will also examine the UT variation of the equivalent current function and the scalar magnetic field above the ionosphere from TIEGCM and CM3e and discuss our findings.

13.4 MTI.04: Implementation of the ionospheric E-region in the Sheffield University Plasmasphere-Ionosphere Model. by Terra, Pedrina

Status of first author: student not in poster competition PhD

Authors: P.M.S. Terra, Instituto Nacional de Pesquisas Espaciais, INPE, pedrina@dae.inpe.br; J.R. deSouza, Instituto Nacional de Pesquisas Espaciais, INPE, jonasdesouza@cc.usu.edu; G.J. Bailey, Space and Atmospheric Group, University of Sheffield, G.bailey@sheffield.ac.uk; J.H.A. Sobral, Instituto Nacional de Pesquisas Espaciais, INPE, sobral@dae.inpe.br; C.G.M. Brum, Instituto Nacional de Pesquisas Espaciais, INPE, garnett@dae.inpe.br

Abstract: The Sheffield University Plasmasphere-Ionosphere Model (SUPIM) has been enhanced to include the ionospheric E-region. It has implemented additional chemical reactions, three additional wavelength bands, which are important for the E-region, and their photoionization and photoabsorption cross sections. In addition, in this version of SUPIM, we have used the extreme ultraviolet and ultraviolet solar fluxes from the SOLAR2000 model [<http://SpaceWx.com>]. Results obtained from the enhanced model have been compared with the experimental digisonde data obtained at Cachoeira Paulista (22.5 S, 45W, dip 30 S) during periods of solar maximum and minimum activities.

14 Wednesday Evening 18 June 2003 Poster Session Abstracts, Equatorial thermosphere and ionosphere

14.1 EQU.01: Characterization of Low-Latitude Ionospheric Plasma Depletions Using Space-Based Ultraviolet Imaging by Comberiate, Joseph

Status of first author: student in poster competition PhD

Authors: Joseph Comberiate, University of Illinois, comberia@uiuc.edu Farzad Kamalabadi, University of Illinois, farzadk@uiuc.edu Larry Paxton, JHU/APL Larry.Paxton@jhuapl.edu Hyosub Kil, JHU/APL Hyosub.Kil@jhuapl.edu

Abstract: Modeling and characterization of ionospheric structures and dynamics are important issues in aeronomy. Recently the Global Ultraviolet Imager (GUVI) on-board the Thermosphere Ionosphere Mesosphere Energetics and Dynamics (TIMED) satellite has detected far ultraviolet (FUV) images of plasma depletions in the low-latitude and equatorial ionosphere. A model of GUVI observation geometry was developed to simulate radiance observations of a model ionosphere. Refinements have been made to this model to enhance its ability to realistically characterize observations of plasma depletions. We report on improved results in reconstructing multi-dimensional electron density profiles from GUVI brightness measurements through the use of statistical inversion techniques. Case studies and comparisons with overlapping data sets are presented as a means of validation of these results.

14.2 EQU.02: Post-Sunset Equatorial Plasma Bubbles During Geomagnetic Storms by Habash Krause, Linda

Status of first author: non-student

Authors: L. Habash Krause (Linda.Krause@usafa.af.mil), USAF Academy H. Dogo (C03Harun.Dogo@usafa.af.mil), USAF Academy

Abstract: Plasma density data from the Defense Meteorological Satellite Program (DMSP) F-14 satellite have been used in conjunction with the Disturbance Storm Time Index (Dst) and the Polar Cap Index (PCI) to obtain a correlation between equatorial plasma bubbles and electric fields associated with various forms of magnetospheric activity. Thirty post-sunset events in 1998 were analyzed; plasma bubble depth ($d = \log_{10}(n_{\text{ambient}}/n_{\text{bubble}})$) varied from 0.2 to 2.2 for this data set. Deep bubbles ($d \geq 1$) were observed exclusively during the main phase of strong magnetic storms (minimum Dst ≤ -60 nT). Impulsive increases in PCI observed during this time indicate favorable conditions for penetration of eastward electric fields to the equatorial ionosphere before sufficient development of the shielding ring current. Some moderate plasma bubbles ($d \approx 1$) were accompanied by sustained fluctuations in PCI, possibly indicating electric field penetration due to a break in shielding associated with a fluctuating polar convection electric field. Shallow bubbles ($d < 1$) were often observed during the recovery phase of magnetic storms varying in strength (minimum Dst from -30 nT to -210 nT). Coincident fluctuating PCI and Dst indicate shallow bubbles may be prevalent during substorm activity.

14.3 EQU.03: Equatorial plasma depletions: large-scale structure and scintillation by Hei, Matthew

Status of first author: student in poster competition PhD

Authors: Hei, M.A., University of Texas at Dallas, matthei@utdallas.edu Heelis, R.A., University of Texas at Dallas, heelis@utdallas.edu McClure, J.P., University of Texas at Dallas, mcclure@utdssa.utdallas.edu

Abstract: Previous studies of the seasonal and longitudinal occurrence of equatorial plasma depletions have used the S4 scintillation index and $\delta n/n$ as indicators of bubble activity. It is possible, however, that

the S4 index is affected by the background density and bubble packing density (number of bubbles per unit volume). Differences in scintillation-based occurrence patterns and $\Delta n/n$ based patterns may be caused by these additional influences. We characterize the large-scale properties of depletion regions found within the AE-E number density database, including the critical parameters of background density and bubble packing density. By extracting this information, we are able to examine seasonal and longitudinal variations that may reconcile existing descriptions of scintillation and bubble occurrence.

14.4 EQU.04: A Study of the Seasonal Variation of the Low-Latitude Ionosphere by Lin, Charles

Status of first author: student in poster competition PhD

Authors: C. H. Lin, High Altitude Observatory, National Center for Atmospheric Research, Boulder, Colorado, USA Institute of Space Science, National Central University, Chung-Li, Taiwan
G. J. Bailey, Department of Applied Mathematics University of Sheffield, Sheffield, UK
A. D. Richmond, High Altitude Observatory, National Center for Atmospheric Research, Boulder, Colorado, USA

Abstract: The Sheffield University Plasmasphere-Ionosphere Model (SUPIM) is used to study the Equatorial Ionization Anomaly (EIA) of the low latitude ionosphere during the solar maximum condition. It is found that the electron density and the location of EIA peaks in both hemispheres show prominent seasonal variations. We present the model simulated density profile, plasma flux, and the total electron content (TEC) along the longitudinal sector of 120° E. The model calculated TEC agrees well with GPS TEC measurement at this longitudinal sector and it generally characterized by (1) in solstice, only the EIA peak in the winter hemisphere remains and a comparatively weak EIA density structure appears in the summer hemisphere, (2) in equinox, two EIA peaks are manifest and the overall electron density is larger than in solstice, (3) in the southern EIA region, the decrease of the electron density in solstice is not as obvious as in the northern EIA region because of the offset of the magnetic equator and the geographic equator. The asymmetry of the EIA peak in solstice is mainly due to asymmetric plasma flux flow from the summer hemisphere to the winter hemisphere and the so called winter anomaly effect. We also examine the plasma flux, plasma production and loss to clarify the importance of the plasma transport in comparison with the seasonally dependent ionization production and loss. Finally, we present the results of the model runs that replace the neutral wind patterns of the empirical neutral wind model originally in SUPIM by the NCAR Thermosphere-Ionosphere Electrodynamics General Circulation Model (TIEGCM).

14.5 EQU.05: Post-sunset equatorial irregularities and magnetic storms by Martinis, Carlos

Status of first author: student in poster competition PhD

Authors: Carlos Martinis, Boston university, martinis@bu.edu Michael Mendillo, Boston University, mendillo@bu-ast.bu.edu Jules Aarons, Boston University, aarons@bu-ast.bu.edu

Abstract: Geomagnetic storms can affect significantly the dynamics of the low latitude ionosphere. Neutral composition, neutral winds, plasma drifts and equatorial irregularities (ESF) are some of the parameters that respond to geomagnetic activity. Past studies made the distinction between magnetically active and quiet periods on the basis of Kp, Ap or Dst indexes for the day. Attempts to correlate the occurrence or inhibition of equatorial irregularities with geomagnetic activity have produced seemingly contradictory results. We apply an empirical vertical drift model, based on Jicamarca data and the AE index, to the post-sunset development of equatorial irregularities during two magnetic storms. Both the successful aspects and the difficulties involved will be outlined. GPS and DMSP data are used to determine the development of irregularities throughout the equatorial region. We confirm the importance of the relation between geomagnetic storm time and local time at a given longitude.

14.6 EQU.06: Horizontal Density Gradient as an Indicator for the Subsequent Occurrence of Equatorial Spread-F Irregularities Along a Satellite Track at 600 km Altitude by Su, Shin-Yi presented by Ho,Hsu-Hui

Status of first author: non-student

Authors: S.Y,Su ; Institute of Space Science, National Central University, Chung-Li, Taiwan, Center for Space and Remote Sensing Research, National Central University, Chung-Li, Taiwan ; t2700146@ncu865.ncu.edu.tw H.H,Ho ; Institute of Space Science, National Central University, Chung-Li, Taiwan ; hshui@csrsddc.csr.sr.ncu.edu.tw C.K,Chao ; Institute of Space Science, National Central University, Chung-Li, Taiwan ; ckchao@jupiter.ss.ncu.edu.tw C.H,Liu ; Institute of Space Science, National Central University, Chung-Li, Taiwan, Dept of Communication Engineering, National Central University, Chung-Li,Taiwan ; chliu@cc.ncu.edu.tw

Abstract: Since activated on March 20, 1999, the Ionospheric Plasma and Electrodynamics Instrument (IPEI) onboard the first satellite of the Republic of China, ROCSAT-1 has continuously collected the global ion distribution data at 600 km altitude between latitudes ± 35 degrees during the solar maximum years of 1999, 2000, 2001, and 2002. Equatorial spread-F (ESF) density irregularities observed with this large amount of ion dataset have been used to study the occurrence statistics of the ESF events. The global and local-time distributions of the ESF occurrence as well as the occurrence dependence on the magnetic conditions are found to be similar to what has been published in the literature except that the statistics of the local-time distribution of the ESF occurrence for various magnetic conditions is now available. Furthermore, based on the previous studies that the existence of a large vertical drift velocity which results in a higher F-peak is the key factor in causing the ESF events, relationship between the horizontal density gradient and the subsequent ESF occurrences at a later time along the ROCSAT orbit is examined. The density gradient in density deviation from a seasonal averaged background level can be served as an indicator to predict the occurrence and non-occurrence of the ESF events along the satellite track. A success rate between 70% and 85% for any month in the year 2000, 2001, and 2002 has been achieved by choosing a threshold in the density gradient to predict either occurrence or non-occurrence of the ESF events later along the same orbit.

14.7 EQU.07: The Seasonal and Local-time Variations of the Global Topside Ionospheric ion Density at 600 km Altitude and its Relationship to the Occurrence Rate of the Equatorial Spread-F Irregularities by Su, Shin Yi presented by Huang, Chiung Huie

Status of first author: non-student

Authors: Shin Yi Su: 1.Institute of Space Science, National Central University, Chung-Li, Taiwan
2.Center for space and Remote Sensing Research, National Central University, Chung-Li, Taiwan
t2700146@ncu865.ncu.edu.tw
Chiung Huie Huang: 1.Institute of Space Science, National Central University, Chung-Li, Taiwan
chhuang@csrsddc.csr.sr.ncu.edu.tw
C. K. Chao: 1.Institute of Space Science, National Central University, Chung-Li, Taiwan
ckchao@jupiter.ss.ncu.edu.tw
H. C. Yeh: 1.Institute of Space Science, National Central University, Chung-Li, Taiwan
yeh@jupiter.ss.ncu.edu.tw

Abstract: The seasonal, longitudinal/latitudinal, and local-time variations of the topside ionospheric ion density observed by ROCSAT-1 at 600 km altitude have been analyzed for the solar activity effects during the solar maximum years of 1999, 2000, and 2001. The ion density level at 600 km altitude has been found to vary with the solar flux index. However, it is noted that the increased density enhancement displays a more prominent increase at the crest than at the trough of the equatorial ionization anomaly (EIA) during the year of high solar activity. Although such enhancement of the EIA feature is related to the enhanced eastward electric field of F-region dynamo, there seems no apparent increase in occurrence rate of the related equatorial spread-F irregularity events. Individually, every enhanced eastward electric field will increase

the F-region peak in which the related upward drift will increase the occurrence of the ESF irregularities. Statistically, the prolonged eastward electric field activity from high solar activity does not increase the probability of the ESF occurrence.

14.8 EQU.08: Statistics of equatorial Spread F activity during the June solstice in the American sector by Valladares, Cesar

Status of first author: non-student PhD

Authors: Cesar E. Valladares Boston College valladar@bc.edu Jorge Chau Jicamarca Radio Observatory chau@geo.igp.gob.pe

Abstract: In the last 40 years, different observing techniques have demonstrated that during the June solstice the occurrence of ESF in the American sector is minimum. This paper attempts to investigate the background ionospheric conditions that favor the formation of ESF irregularities during this season. Measurements of UHF scintillations at Ancon conducted during the last 9 years have corroborated that in fact scintillation activity during the June solstice developed only an average of 10% throughout the last solar cycle. We found that the occurrence of ESF presents significant solar cycle, and Kp dependencies and a tendency for scintillations to appear at later local times (near midnight). For low Kp values scintillations are about 20% during solar min, but diminish to 5% during solar max. For disturbed magnetic conditions, there exists a 40% occurrence of scintillations during solar max, but is less for solar min conditions. We have used radar maps collected by the JULIA radar during 39 nights during the months of June and July 2002. During this period only 1 night, July 5, 2002, presented well-developed plumes, which coincided with TEC depletions and UHF and GPS scintillations. On nine other nights the JULIA radar detected bottom-type echoes. Simultaneously with the ESF observations, bottomside density profiles were measured by the Jicamarca digisonde and TEC latitudinal profiles were reconstructed using a latitudinal network of 10 GPS receivers. We present the patterns of TEC and density profiles for the few nights of UHF scintillations and radar plumes and compare these with the climatology and variability of the density and TEC distributions for nights of no ESF. We also show results of numerical simulations of the low latitude ionosphere using the IFM model and different drivers to reproduce the hemispherical asymmetry that characterizes the TEC latitudinal profiles during the June solstice and the ionospheric characteristics that predominate during days when ESF develops.

14.9 EQU.09: Longitude variations in topside equatorial ionospheric parameters and comparisons with ground based radars by Venkatraman, Sarita

Status of first author: non-student

Authors: Sarita Venkatraman, University of Texas at Dallas, sarita@utdallas.edu
Rod Heelis, University of Texas at Dallas, heelis@utdallas.edu
Dave Hysell, Cornell University, daveh@geology.geo.cornell.edu

Abstract: Comparison of topside equatorial parameters obtained from DMSP satellites with those measured from Jicamarca radar demand that a common volume bounded in latitude, longitude, and altitude be defined.

To determine acceptable limits for this volume, knowledge of the spatial gradients in the parameters must be defined. Those can be obtained independently from each data source and are dependent on local time and season. Having described the spatial gradients, a comparison of the ionospheric variables can be made. The present study focuses on simultaneous ground based and satellite data obtained for June 2002. Data for days 11, 12, and 13 are compared in this study. Satellite data are obtained from the DSMP satellites F13 (0600 - 1800 LT) and F15 (0900 - 2100 LT) respectively. Ground based data are obtained from the Jicamarca radar.

15 Wednesday Evening 18 June 2003 Poster Session Abstracts, Instruments/techniques for thermosphere and ionosphere observations

15.1 ITI.01: New All-Sky Imager and Microbarograph at Arecibo Supports CEDAR Community. by Farias Gutierrez, Paloma

Status of first author: student not in poster competition Masters

Authors: Paloma Farias Gutierrez Communications and Space Sciences Laboratory The Pennsylvania State University pgf110@psu.edu

Johannes Wiig Communications and Space Sciences Laboratory The Pennsylvania State University jaw972@psu.edu

Dr. John D. Mathews Communications and Space Sciences Laboratory The Pennsylvania State University jdmathews@psu.edu

Abstract: A description is given of the new web-available, state-of-the-art all-sky imager and microbarograph deployed at the Arecibo Observatory (AO) by the Communications and Space Science Laboratory of the Pennsylvania State University. We give an exposition of the method used to image the lower F-region above AO in combination with local barometric pressure. The interactive website for these instruments is also introduced. The website allows near real time data access, analysis, archive searches, and data downloading.

15.2 ITI.02: Preliminary Analysis of Data Gathered from the New All-sky Imager and Micro-barograph System at AO. by Wiig, Johannes

Status of first author: student not in poster competition Masters

Authors: Johannes Wiig Communications and Space Sciences Laboratory The Pennsylvania State University jaw972@psu.edu

Paloma Farias Gutierrez Communications and Space Sciences Laboratory The Pennsylvania State University pgf110@psu.edu

Dr. John D. Mathews Communications and Space Sciences Laboratory The Pennsylvania State University jdmathews@psu.edu

Abstract: A status report is given on the on-going program for monitoring the various upper atmosphere airglow features with the all-sky imager system and microbarograph. These instruments have been newly installed at the Arecibo Observatory by the Communications and Space Science Laboratory of the Pennsylvania State University. A presentation of the data acquired from the system is given with the ultimate goal of investigating the possible relationships between acoustic gravity waves, ion rain, and ocean swells.

15.3 ITI.03: Observation and Analysis of Whistler Mode Echoes Received by RPI on IMAGE at High Latitudes by Chen, Xiangdong

Status of first author: student in poster competition PhD

Authors: X. Chen, Clemson University, xchen@clemson.edu V. S. Sonwalkar, University of Alaska Fairbanks, ffvss@uaf.edu

Abstract: Whistler-mode wave-injection experiments with Radio Plasma Imager (RPI) on IMAGE offer an opportunity to observe the whistler-mode echoes. We have performed raytracing studies to investigate accessibility of whistler-mode waves injected from IMAGE to various regions of the magnetosphere and also to other satellites such as Akebono. RPI detected both discrete and diffuse whistler-mode echoes during our observing period (April 21 to August 28, 2000) when IMAGE was at a low altitude (1000-7000 km) and mid-to-high latitude ($\geq 25^\circ$ - 40° S) near its perigee. We believe that the discrete echoes are the result of RPI signals reflected at the Earth-ionosphere boundary and the diffuse echoes are the result of scattering

of RPI signals by meter-scale irregularities. Raytracing analysis shows that both ducted and nonducted ray propagation are needed to explain the observed whistler-mode dispersion. Comparison of electron densities obtained from our raytracing analysis of dispersion with the electron densities obtained by Kletzing et al. in the Auroral Zone shows that these density values deduced from RPI data were about ten times higher. This may be because the antenna radiation efficiency is higher at higher electron densities.

15.4 ITI.04: Instrumentation upgrade for Fabry-Perot studies of equatorial thermospheric dynamics and composition by Chen, Xiangdong

Status of first author: student in poster competition PhD

Authors: X. Chen, Clemson University, xchen@clemson.edu J. Meriwether, Clemson University, meriwj@ces.clemson.edu M. Biondi, University of Pittsburgh, biondi+@pitt.edu P. Sherwood, Interactive Technology, Inc. iti@world.std.com

Abstract: Fabry-Perot technology has progressed to the point where significant gains in sensitivity can be achieved by the replacement of the GaAs phototube detector with a CCD digital camera. Calculations demonstrate a gain in sensitivity of a factor of 15 may be achieved. We would therefore expect a reduction in the standard deviations of the horizontal wind component from 10 m/s to 5 m/s and for temperature from 40-50 K to 10-15 K for a signal brightness of 100 Rayleigh and an integration period of 10 to 15 minutes. The automated Arequipa Fabry-Perot interferometer (FPI) observatory operating at Arequipa, Peru (16.47S, 71.49W), is undergoing an upgrade represented by the detector replacement of the GaAs phototube with a low noise back-thinned Andor Technology CCD camera. This upgrade features the replacement of the CAMAC electronics with a PC-based interface. The data acquisition software is being upgraded with a suite of C/C++ programs (MASTER, CAMERA, OBSERVATORY, DISPLAY/ANALYSIS) written by Interactive Technology that operate as separate, communicating, processes. As part of this upgrade we have also included a filter changer to enable observations of the spectral profile of the O+ 732 emissions during evening and morning twilights to infer Doppler broadening and Doppler shifts for the ionospheric component of the thermosphere region at altitudes between 200 to 500 km. During the night observations of mesospheric winds would be achieved by observing the Doppler shift of the OH P1(2) line at 731.6 nm with the 732 nm filter. Finally we plan to observe the 630 nm thermospheric airglow emission with a second Fabry-Perot observatory located at Huancayo, Peru. Simultaneous measurements of thermospheric winds in a common volume between Arequipa and Huancayo regions of Peru from two different directions (East from Huancayo, North from Arequipa) would produce a measurement of the complete thermospheric wind vector in the thermosphere within a volume that is about 50 km square and 100 km thick. These results would be studied for variations caused by the propagation of thermospheric gravity waves. The testing of the Andor camera and data acquisition software is nearing completion, and we expect installation to take place during the summer of 2003.

15.5 ITI.05: SOFDI: An Update on Instrument Development, Forward Model, and Inversion Algorithms by Gerrard, Andrew

Status of first author: non-student

Authors: Andrew J. Gerrard Clemson University and SUNY Morrisville gerraraj@morrisville.edu
John W. Meriwether Clemson University john.meriwether@ces.clemson.edu
Paul Hayes Michigan Aerospace Corporation hays@michiganaerospace.com
Carl A. Nardell Michigan Aerospace Corporation cnardell@michiganaerospace.com

Abstract: Daytime measurements of winds and temperatures based on the 630 nm emission from thermospheric atomic oxygen (OI) have been difficult to obtain because of the large solar background continuum which overpowers the comparatively weak emission. Though measurements of this dayglow transition have been attempted by a number of different groups in the past, the scientific significance of these measurements has been somewhat limited in scope. However, the Second generation Optimized Fabry-Perot Doppler Imager (SOFDI), based on the design of the UARS HRDI instrument, makes use of a number of innovative

optical techniques which will allow for day and night measurements of the 630 nm line, as well as the 557 nm transition of OI, the 732 nm transition of O+, and the 840 nm 6-2 P1(2) rotational line of OH, and others. These results are expected to yield a wealth of information for the aeronomy community, including the mapping of the dayglow and nightglow thermospheric horizontal and vertical winds, study of the 630 nm dayglow brightness distribution as applied to the Appleton anomaly formation, 732 nm observations of ion temperatures and ion drifts during morning or evening twilight, measurements of the variability of thermospheric atomic oxygen concentrations, the investigation of possible hot oxygen at low latitudes, the determination of OH rotational temperature and winds, observations of the full diurnal variation of thermospheric temperature and winds, etc. As such, as part of the SOFDI initiative, it is the purpose of this paper to present 1) an up-to-date summary of the construction of the SOFDI instrument and 2) an overview of the instrument forward model and associated inversion algorithms based on theoretical calculations. It is shown that the construction of the SOFDI instrument is preceding as scheduled, and will be ready for test runs in early July 2003 in upstate New York. In addition, we show that the data analysis infrastructure is currently being optimized based on results from the forward model. We expect that by late August/early September, the SOFDI instrument will be ready for scientific data collection.

15.6 ITI.06: A Microcontroller based Generic Radar Controller by Kolatkar, Aditi

Status of first author: student in poster competition Masters

Authors: Aditi Kolatkar University of Alaska, Fairbanks ftabk@uaf.edu
Denise Thorsen University of Alaska, Fairbanks ffdt@uaf.edu

Abstract: Increasingly radar stations contain multiple radar systems, each individually controlled. Non-standard control requires that a user of multiple systems learn each system separately. Additionally, multiple radar controllers make coordination of multiple systems difficult. The Remote Sensing Lab at University of Alaska Fairbanks, is building a generic radar controller that can be used to operate any pulsed radar system or multiple radar systems simultaneously. Technicians at radar stations where this controller is deployed will only need to know how to operate a single system rather than many. Additionally, campaigns using multiple radars can be coordinated through a single radar controller. The University of Alaska generic radar controller is a microcontroller based PC card with a minimum of 16 control pulses. Each pulse can be individually programmed is intended to provide pulses of 100 ns duration upto several milliseconds and variable pulse repetition intervals.

15.7 ITI.07: Application of Neural Network for Ionospheric Data Assimilation and Forecasting by Mantz, Chris

Status of first author: student in poster competition Undergraduate

Authors: Chris Mantz (Mantzcp@muohio.edu), Qihou Zhou (ZhouQ@muohio.edu), Yu T. Morton (Mortonyt@muohio.edu) School of Engineering and Applied Sciences Miami University Oxford, Ohio
Mike Sulzer (Sulzer@naic.edu) Arecibo Observatory Arecibo, Puerto Rico

Abstract: The flexibility and versatilities of neural networks have made them an important tool for data assimilation and decision makings. This poster explores the application of neural network to assimilate the data collected by the Arecibo incoherent scatter radar (ISR) over two decades. Our model inputs include date, local time, solar radiation index, geomagnetic index and other pertinent variables. Our outputs include all the F-region parameters measured by the Arecibo ISR. We investigate various neural network architectures to find out the most suitable one for our application.

15.8 ITI.08: A new lagprofile based approach to the inversion of incoherent scatter radar data by Nikoukar, Romina

Status of first author: student in poster competition PhD

Authors: Romina Nikoukar, University of Illinois, nikoukar@uiuc.edu Farzad Kamalabadi, University of Illinois, farzadk@uiuc.edu Erhan Kudeki, University of Illinois, e-kudeki@uiuc.edu Michael Sulzer, NAIC, msulzer@naic.edu Sixto Gonzalez, NAIC, sgonzalez@naic.edu

Abstract: This work investigates optimal inversion techniques pertaining to the extraction of ionospheric parameters such as altitude profiles of electron density, electron temperature, ion temperature, hydrogen and helium ion fraction ratio. The conventional methods currently used for the inversion process suffer from complicated data preprocessing and computational issues. Among these approaches lag-profile techniques require much less data preprocessing. Computational issues to achieve a satisfactory spatial resolution, however, remain a major challenge.

The proposed method exploits the simple data preprocessing of the lag-profile approaches. Moreover, it reduces the computational complexity by introducing a two-step inversion process. Computation of ionospheric autocorrelation function (ACF) from a set of 1-D deconvolutions forms the first step, while estimation of the ionospheric parameters based on the obtained ACFs is performed in the second step. Experiments show promising results which are superior to conventional inversion methods regarding computational complexity and spatial resolution.

15.9 ITI.09: Identification of Ionospheric Sporadic E using Fuzzy Equivalence Techniques by SIKDAR, PAYEL

Status of first author: student in poster competition Masters

Authors: PAYEL SIKDAR, GRADUATE STUDENT, UTAH STATE UNIVERSITY, LOGAN, UT
EMAIL: payel@cc.usu.edu
Dr. FRANK T. BERKEY RESEARCH PROFESSOR, DEPARTMENT OF PHYSICS, UTAH STATE UNIVERSITY, LOGAN, UT EMAIL: ftb@cc.usu.edu

Abstract: A new approach to analyze ionograms for the presence of ionospheric sporadic-E layers is proposed here. It is based on the concepts of fuzzy-equivalence, which define a relation that is reflexive, symmetric and max-min transitive. The approach that is employed entails the use of a sliding window for clustering data points, where the clusters in successive windows are grouped by the transitive property of equivalence. The algorithm is computationally more efficient than analyzing all the points in the complete data set at once. Principle component analysis is applied for curvature estimation and the various Es layers are thus identified. In this paper, the analysis has been applied to digital ionograms acquired from the dynasonde operated at the USU Bear Lake Observatory.

15.10 ITI.10: Calculating induced electric and magnetic fields near coastal regions by Simon, Shepherd

Status of first author: non-student

Authors: Simon G. Shepherd, Fridon Shubitidze, and William Lotko Thayer School of Engineering, Dartmouth College, Hanover, NH simon.shepherd@dartmouth.edu

Abstract: Geomagnetically induced currents (GICs) are a potentially damaging space weather phenomenon that are caused primarily by time-varying electric currents in the high-latitude ionosphere due to substorms and geomagnetic storms. Modeling GICs involves determining the induced electric field at the surface of the Earth, which requires detailed knowledge of both the primary source currents and the conductivity structure of the underlying geology. Most present techniques for calculating the induced electric (and magnetic) fields are incapable of handling horizontally inhomogeneous conductivity structure and are, therefore, inaccurate in regions with large conductivity gradients, such as in coastal regions. A technique that is not restricted in this manner, the method of auxiliary sources (MAS), is used to calculate the fields in several 1D Earth models. It is shown that the MAS is more accurate than standard techniques. The induced electric and magnetic fields are also calculated using a 2D model of the land/ocean interface to demonstrate the geomagnetic coastal effect (GCE), as it is known in the solid Earth community, and to illustrate the importance of including such structure when modeling geomagnetic induction in coastal regions.

15.11 ITI.11: Effects of hot oxygen on midlatitude ground-based Fabry-Perot temperature measurements by Sipler, Dwight

Status of first author: non-student

Authors: Dwight Sipler MIT Haystack Observatory dsipler@haystack.mit.edu
Manfred Biondi University of Pittsburgh biondi+@pitt.edu

Abstract: The response of a ground-based Fabry-Perot interferometer (FPI) to predicted non-Maxwellian energy distributions of atomic oxygen in the F-region is calculated. Analysis of the simulated profiles shows that the high energy component of the non-Maxwellian profiles has a modest effect on ground-based measurements, raising the temperature derived from the Doppler-broadened profiles above that of the thermosphere in the 630 nm emission region. The effect is small compared to the uncertainties for an individual measurement but could be significant when large numbers of profiles are averaged in an attempt to reduce uncertainties in the determinations. However, the effect can not account for the $\sim 100\text{K}$ difference between the FPI determinations and values derived from empirical models such as MSIS.

16 Wednesday Evening 18 June 2003 Poster Session Abstracts, Data visualization and management

16.1 DVM.01: The CEDAR Database by Barnes, Roy

Status of first author: non-student

Authors: Roy Barnes (bozo@ucar.edu) NCAR/HAO, Jose Garcia (jgarcia@ucar.edu) NCAR/HAO, Jimin Wang (jiwang@ucar.edu) NCAR/HAO, Barbara Emery (emery@ucar.edu) NCAR/HAO, Peter Fox (pfox@ucar.edu) NCAR/HAO

Abstract: Coupling, Energetics and Dynamics of Atmospheric Regions (CEDAR) is a program sponsored by the National Science Foundation (NSF) to enhance the capability of ground-based instruments to measure the upper atmosphere and to coordinate instrument, model and geophysical index data for the benefit of the scientific community. The CEDAR Database at HAO/NCAR is the central repository for data from 13 instrument classes of radars and optical instruments, as well as geophysical indices, empirical models and output from large models. The CEDAR Database is the ground-based part of the TIMED/CEDAR Data System, and is also accessible via the Space Physics and Aeronomy Research Collaboratory (SPARC). The data are accessed via the web at <http://cedarweb.hao.ucar.edu>. We will highlight our present access and graphics capabilities, and welcome comments on areas of improvement for users.

16.2 DVM.02: Road map of the TIMED Science Data System web site by Nylund, Stuart

Status of first author: non-student

Authors: Stuart Nylund, JHU/APL, Stuart.Nylund@jhuapl.edu Paul Lafferty, JHU/APL, Paul.Lafferty@jhuapl.edu

Abstract: The Thermosphere Ionosphere Mesosphere Energetics and Dynamics (TIMED) Science Data System (SDS) is a distributed system responsible for the acquisition, generation, distribution, and archive of science data necessary to support the TIMED mission. The major elements of the SDS are dispersed across several different facilities: the Mission Data Center (MDC) - the facility responsible for telemetry distribution and other central functions; and four Payload Operations Centers (POC) - remote facilities responsible for TIMED instrument data operations of data reduction, processing and distribution of data analysis products. Additionally, through support furnished primarily by CEDAR, collaborating ground-based investigators make data available to the SDS. The SDS provides a user interface, implemented as a World Wide Web (Web) site, to permit TIMED investigators, the scientific community and the general public to locate, understand and use this collection of data - now continuously covering over 16 months.

The major features of the TIMED SDS Web site for coordinated observation planning, information access, and data query and retrieval are presented. Illustrations show how to navigate and use the various resources of the site. Example results are given to highlight these features and capabilities.

16.3 DVM.03: Advances in the Madrigal Database by Rideout, William

Status of first author: non-student

Authors: William Rideout (brideout@haystack.mit.edu), MIT Haystack Observatory, John Holt (jmh@haystack.mit.edu), MIT Haystack Observatory, A van Eyken (Tony.van.Eyken@eiscat.com), EISCAT Scientific Association, Kiruna, Sweden

Abstract: The Madrigal database is a web application designed to allow easy access to distributed upper-atmosphere data. Since the data is stored locally at the various Madrigal installations, it can be updated easily as data analysis methods are improved; but since all the sites are linked, data from all sites can be searched for at once. Madrigal is an open-source project - its code can be freely downloaded and improved by anyone in the community.

The main purpose of this poster is to publicize various recent enhancements to Madrigal. These include:

- the ability to search the entire database at once using almost any possible filter
- greatly simplified APIs that allow the system to be easily extended in Fortran, C, Matlab, or a number of scripting languages
- improvements in the basic isprint page that allow flat files to be generated using almost any possible filter

A second purpose of this poster will be to gather user-response to Madrigal: how could it be improved? what problems have users had with this web site?

16.4 DVM.04: Web-Based Space Physics Metadata Searching Using Space Physics Data Markup Language by Weiss, Michele

Status of first author: non-student

Authors: Michele Weiss, JHU/APL michele.weiss@jhuapl.edu, Daniel Morrison, JHU/APL daniel.morrison@jhuapl.edu, Larry Paxton, JHU/APL larry.paxton@jhuapl.edu, Robin Barnes, JHU/APL robin.barnes@jhuapl.edu

Abstract: We are developing the Space Physics Data Markup Language (SPDML) using eXtensible Markup Language (XML) to provide a standard method for expressing Space Physics data sets. SPDML is being used to prototype a standard method of remote data querying in a distributed data system enabling multi-instrument comparisons. As a testbed, we are initially using data from the NASA TIMED spacecraft and ground-based SuperDARN radars.

This poster presents how SPDML will be used to describe the structure, semantics and content of any space physics data set in any data format. This allows the construction of metadata from existing data sets in both standard (NetCDF, CDF, etc.) formats and mission specific formats to be processed. Commercial off-the-shelf search engines can then be used to discover and access multiple distributed scientific resources, providing easy cataloging and retrieval of Space Physics data as well as providing a multi-instrument comparison to TIMED data.

16.5 DVM.05: A Virtual Observatory for the Ionosphere Thermosphere and Mesosphere community by Yee, Jeng-Hwa presented by Nylund, Stuart

Status of first author: non-student

Authors: Jeng-Hwa Yee, JHU/APL, Sam.Yee@jhuapl.edu Elsayed Talaat, JHU/APL, Elsayed.Talaat@jhuapl.edu Stuart Nylund, JHU/APL, Stuart.Nylund@jhuapl.edu

Abstract: The ionosphere thermosphere and mesosphere (ITM) community studies an area of the atmosphere that is a transition region between the atmosphere and space, where many important physical and chemical processes change dramatically temporally and spatially. The ITM region is where energetic solar radiation is absorbed, energy input from the aurora maximizes, intense electrical currents flow and upward propagating waves and tides break. As a result, the areas of studies within the ITM community span a wide spectrum of scientific subjects in geophysics and space physics. The relevant data for the community collected during the past few decades consequently come from a variety of sources including ground and space-based instruments as well as from modeling and data assimilation. As the different sub-fields mature, a system-oriented approach to understand the ITM as a whole and its relationship to the sun and the surrounding geospace environment is critical. This approach requires efficient access to all data sets (present and historical) relevant to disciplines across agencies, including NASA, NSF, NOAA and others. One of the data systems to be considered is a NASA Sun-Earth Connections Virtual Observatory - the prototype Virtual Solar Observatory. There clearly is a need for a data system to not only serve the ITM community but also to integrate cross-discipline studies with other programs such as CEDAR and GEM.

A preliminary VIO concept is presented based on a set of principles: centralized browse and query/retrieval of distributed resources, access to data reader software and other tools, and integration of current data with data from previous missions and long-term data sets. Drawing upon the design of the Virtual Solar

Observatory (VSO), the VIO concept is expanded to meet the needs particular to the ITM community. It is developed as an introduction to the community for discussion and community-wide input as part of a VIO definition phase. The VSO design is summarized, and the preliminary VIO design is described with its unique characteristics.

Index

- Barnes, Roy, 55
Basu, Sunanda, 35
Bekerat, Hamed , 39
Bishop, Rebecca, 4
Briczinski, Stanley, 27
Brown, Bailes, 6
- Chau, Jorge L., 27
Chen, Xiangdong, 50, 51
Cheng, Zhenggang, 29
Chu, Xinzhao, 2
Comberiate, Joseph, 46
Cosgrove, Russell, 44
- Deng, Yue, 32
Didebulidze, G.G., 10
Drexler, Josef, 39
- Emery, Barbara, 39
Englert, Christoph R., 23
- Faivre, Michael, 23
Fang, Xiaohua, 40
Farias Gutierrez, Paloma, 50
Fernandez, Jose, 1
French, John, 11
Fujii, Junsuke, 11
Fukushima, Tetsuya, 11
- Gardner, L, 41
Gelinas, Lynette, 27
Gerrard, Andrew, 51
Goncharenko, Larisa, 17
- Habash Krause, Linda, 46
Hairston, Marc, 35
Hatch, D., 12
Hei, Matthew, 46
Heinselman, Craig, 44
Herron, Joshua, 4
Hill, Steven, 32
Ho, Hsu-Hui, 48
Huang, Chiung Huie, 48
- Jee, Geonhwa, 35
Johnson, Eric, 41
- Kawahara, Taku, 4
Kawamura, Seiji, 44
Knipp, Delores, 36
Kolatkar, Aditi, 52
Kwak, Young-Sil, 41
- Lehmacher, Gerald , 5
Li, Feng, 12
Li, Tao, 17
Lieberman, Ruth , 17
Lima, Lourivaldo Mota, 18
Lin, Charles, 47
Liu, Ningyu, 29
- Mackler, David, 2
Mantz, Chris, 52
Martinez, Lisandro, 14
Martinis, Carlos, 47
Maruyama, Naomi, 18
Maute, Astrid, 44
Mertens, Christopher, 6
Mierkiewicz, Edwin, 36
Moore, Luke, 32
Moore, Robert, 30
Mutiso, Charles, 19
- Nakamura, Takuji, 11
Nelson, Karen, 19
Nielsen, Kim, 14
Nikoukar, Romina, 52
Nossal, Susan, 37
Nozawa, Satonori, 19
Nylund, Stuart, 55, 56
- Oberheide, Jens, 5
Olsen, Christian, 14
OYAMA, SHIN-ICHIRO, 42
- Pan, Weilin, 5
Peshave, Manasi, 24
Praskovskaya, Eleanor, 24
Praskovsky, Alexander, 25
- Ray, Licia, 28
Remick, Karen, 34
Rideout, William, 55
Ridley, Aaron, 42
Riggin, Dennis M., 6
- Sarango, Martin, 1
Schoendorf, J, 34
Shue, Jih-Hong, 43
SIKDAR, PAYEL, 53
Simon, Shepherd, 53
Sipler, Dwight, 54
Smith, Steve, 15
Snively, Jonathan, 13
SU, LIGUO, 7

Su, Shin Yi, 48
Su, Shin-Yi, 48

Tang, Jing, 13
Taori, A, 20
Terra, Pedrina , 45
Thom, Stuart, 34

Valladares, Cesar, 49
Van Eyken, Tony, 38
Vance, J, 7
Vemula, Sreenivas, 25
Venkatraman, Sarita, 49

Wang, Weiyuan, 25
Weiss, Michele, 56
Wen, Chun-Hsien, 28
Wiig, Johannes, 50
Williams, Bifford, 8
Woodcock, Kenneth, 8
Wrasse, Cristiano, 15
Wright, John, 26
Wrotny, Jonathan, 2
Wu, Qian, 9

Yamamori, Miho, 15
Yee, Jeng-Hwa, 56
Yu, Yonghui, 16
Yuan, Tao, 20
Yue, Jia, 31

Zhang, Shengpan, 21
Zhang, Shengpan , 21
Zhang, Shun-Rong, 38
Zhang, Xiaoli, 22
Zhao, Yucheng, 9